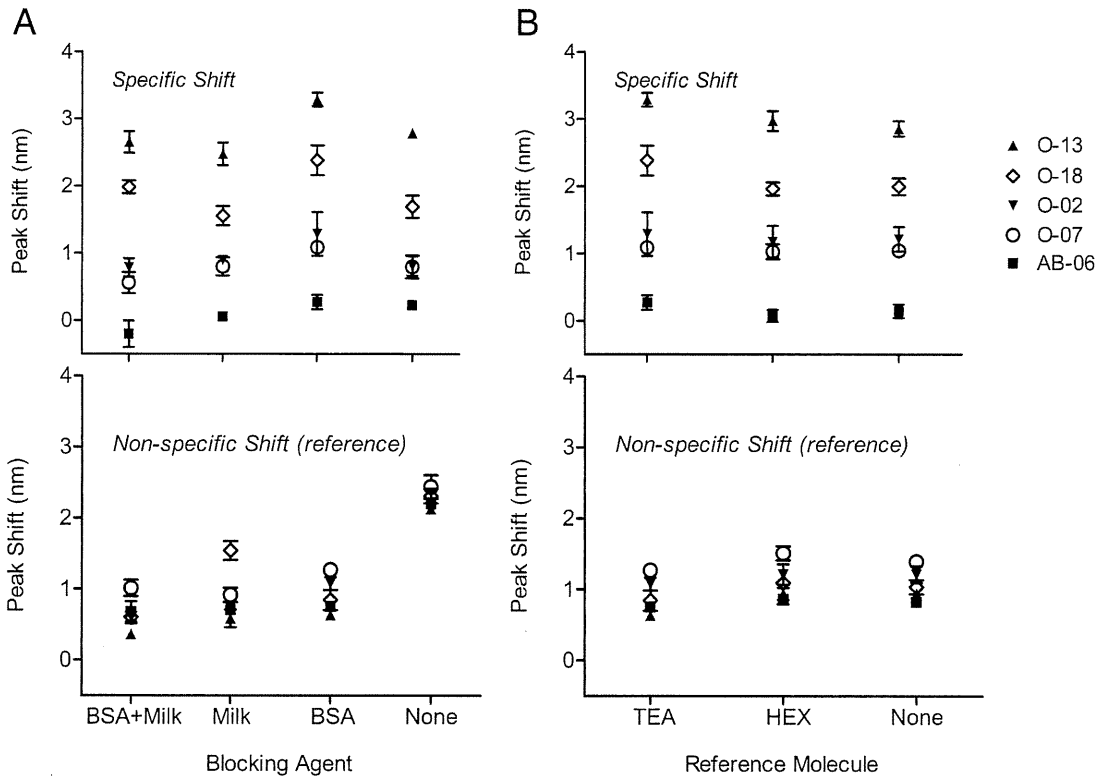

Figure 2. Comparison of effects of blocking agents and reference molecules on sensor responses (shift of λ_{max}). **(A)** Effect of blocking agents: BSA+Skim milk, Skim milk, BSA and None. **(B)** Effect of reference molecules: TEA, HEX and None. The upper graphs represent data from signal wells, whereas the lower graphs represent data from reference wells. Data were acquired using the sera from 4 blood group O and 1 blood group AB volunteers. Error bars represent standard errors.

because we do not expect any response to the blood group A antigen from the serum of blood group AB. We chose the optimum condition for coating as 8.4×10^{-4} % (w/w) at pH 2.0 hereafter, which was in the middle of the stable condition having a large response.

In the second step of the optimization, we further investigated the selection of blocking agents and reference molecules, which would reduce the unknown signals from crude samples and enable a single-step, label-free measurement. We tried well-known blocking agents of BSA, skim milk and their combination. For reference molecules, which were immobilized on the surface of AuNPs in the reference well, we tried TEA and HEX. Based on the result shown in Figure 2, we conclude that choosing BSA and TEA for blocking agent and reference molecule, respectively, can achieve larger signal. Then, we were convinced that the optimum condition of our assay had been achieved and we were ready to proceed to measure various serum samples. Again, we observed a good selectivity towards anti-A antibody also in this optimized condition by using serum of blood group AB.

Validation: Concentration-dependent shifts of λ_{max} by purified human anti-A antibody

We confirmed concentration-dependent shifts of λ_{max} as basic characteristics of our LSPR sensor using purified target antibody: human anti-A antibody (Figure 3). We fitted this profile assuming a 1:1 binding model between anti-A and blood group A antigen. The fitted curve provides us the dissociation constant (K_d) of 1.5×10^{-4} g/mL. Due to the difficulty of preparing a higher concentration of purified anti-A antibody from human blood, we did not measure λ_{max} in a higher concentration range than 40 μg/mL. However, with using the serum that has the highest concentration of anti-A antibody, we observed the similar trend of shifts of λ_{max} across our experimental concentration range.

Challenge: single-step, wash-free measurement of serum samples

We applied our assay to the various samples from volunteers and investigated the applicability of a single-step measurement in crude samples. The difference between the process of "wash" and "wash-free" measurement concerns whether we replace the serum in each well with a buffer solution before performing the spectrum measurement. In the single-step "wash-free" measurement, we do not discard the serum and we proceed directly to the spectrum measurement. The major purpose of this "wash" operation is to significantly reduce the signal from the unknown species in the serum and improve the accuracy of the measurement. Figure 4 compares the signals from both operations. Interestingly, the slope of linear regression between 2 methods is identical to unity with $R^2 = 0.91$. This means that there is no significant difference between them. We therefore conclude that the single-step "wash-free" measurement works

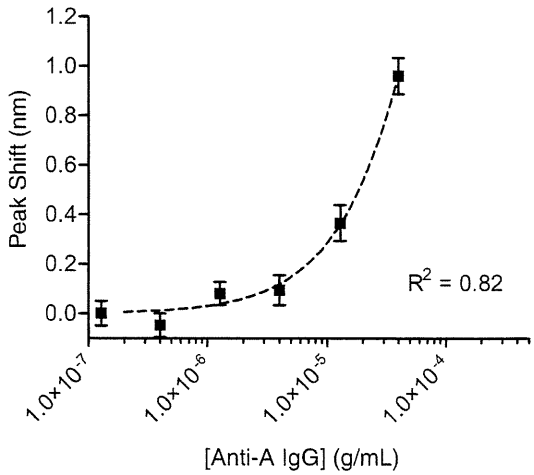

Figure 3. Anti-A concentration-dependent shifts of λ_{max}. Dotted line shows a sigmoidal fitting to the experimental data. Error bars represent standard errors from 8 samples.

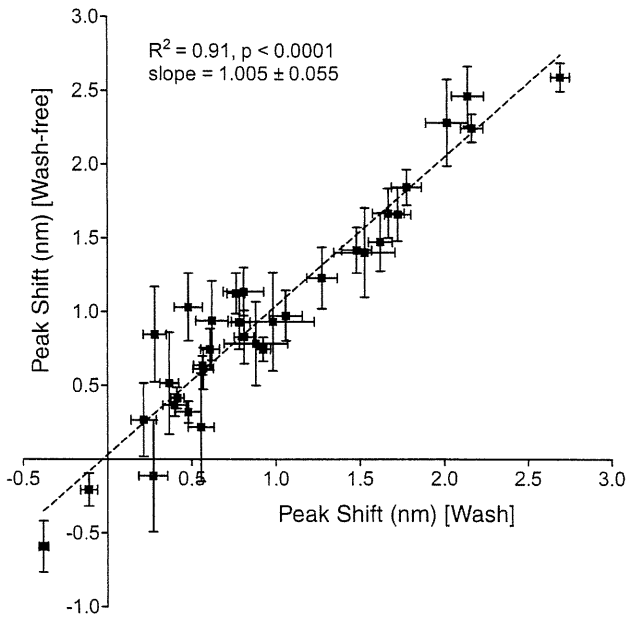

Figure 4. Wash-free measurement. Correlation between "wash-free" and "wash" measurements. Dotted line was determined by linear regression analysis (slope = 1.005, R^2 = 0.91). Error bars represent standard errors.

equivalently to the standard "wash" operation without any significant interference from the serum in the well.

Comparison of the single-step assay with other methods

Finally, we compared our single-step "wash-free" assay with other methods, i.e., TT and SPR, using the common 41 serum samples (Figure 5, *A*). Because two major isotypes of antibodies exist in serum, i.e., IgG and IgM-types, we conducted a supplemental measurement using the secondary antibody (anti-human IgG) that specifically detects the amount of IgG-type anti-A antibody bound on the AuNPs and computed the correlations separately in those two types of measurements (Table 1). As for the TT method, the procedure we used for the computation of correlations is generally assumed to measure IgG-type antibody only. We observed at least moderately strong correlations among the methods. For the IgG-type antibody, the correlation coefficient between LSPR and TT is smaller than that observed between LSPR and SPR (0.66 vs. 0.79). This is possibly due to the less quantitative nature of the TT method, in which results are discrete values. For instance, the TT results of many samples were zero in Figure 5, *B*. On the other hand, correlation coefficients between LSPR and SPR are approximately 0.8 (strong) for both types of measurement, and more than 60% of the variability in the LSPR results is explained statistically by SPR (Figure 5, *A*). In particular, we did not find a difference in the correlations between the measurements of total antibody and IgG-type in the comparison of LSPR and SPR. Thus, we conclude that LSPR and SPR measured the similar types of antibody in our assay because two types of measurements (i.e., total and IgG-type antibody) did not change the correlation between the two methods.

Discussion

Development of a rapid, accurate and sensitive diagnostic method is favored in clinical practices from both financial and ethical points of view. With this goal, many types of new biosensors have been proposed and presented to the clinical community for use in diagnostics. Meanwhile, TT and ELISA have been widely used along with accumulated empirical evidence and increased confidence, even though they require sophisticated operations and substantial time to complete. We believe that one of the tipping points where the clinical community will accept a new method depends on the extent of its simplicity of operation and reproducibility of results relative to the conventional methods.

In this study, we demonstrated a more efficient approach to quantify the amount of antibodies in sera while fulfilling practical requirements. We optimized our assay to detect antibodies in both nano-optical[15] and surface chemical aspects as shown in Figures 1 and 2. The optimal arrangement of immobilized AuNPs and the use of a polyampholytic polymer are two essential elements of our method. The former enhanced the sensitivity and the latter enabled efficient surface chemistry and high selectivity. Though the zwitterionic copolymer looks difficult to control in a stable manner, we found its optimum condition to facilitate surface modification. We believe that larger signal responses using the acidic polymer solution are caused by the dense attachment of the polymer on the surface of AuNPs due to static attraction between positively charged polymer chains and negatively charged AuNPs. The capability of blocking nonspecific binding is similar for BSA and skim milk (Figure 2), but we cannot expect a synergetic effect using both materials simultaneously. From our experience, BSA seems to be a more stable agent for long-term storage. To optimize a reference well, we tried 2 kinds of molecules (i.e., TEA and HEX). As expected, slightly better trends were achieved using more hydrophilic molecules, which have a relatively similar

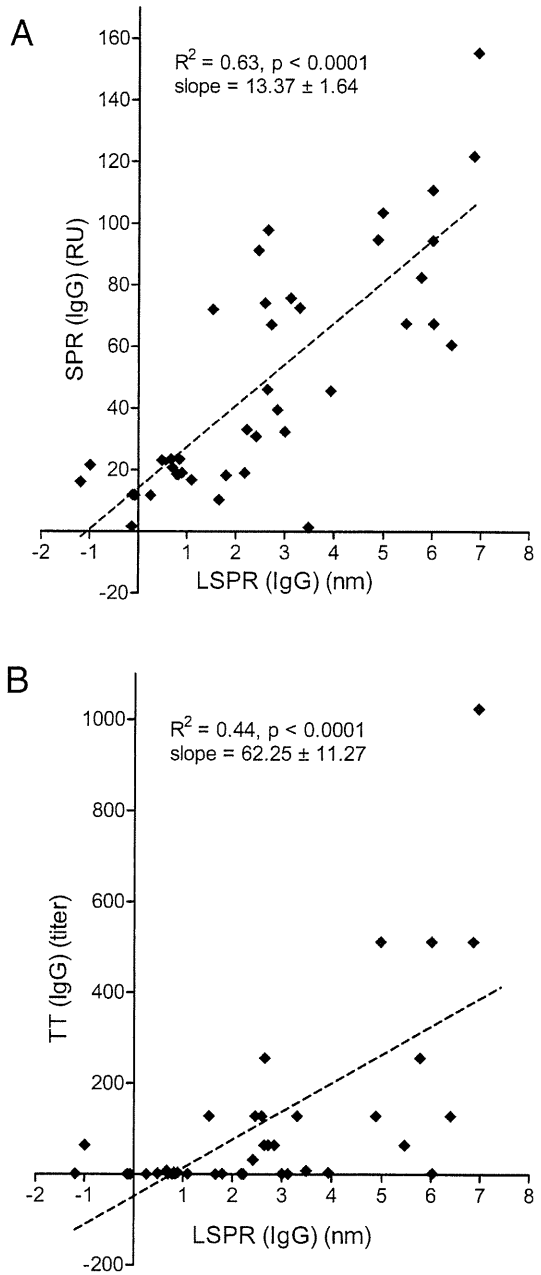

Figure 5. Correlations between TT, SPR and LSPR measurements of 41 volunteers. **(A)** Between SPR (IgG) and LSPR (IgG). Dotted line was determined by linear regression analysis (slope = 13.37, R^2 = 0.63). **(B)** Between TT (IgG) and LSPR (IgG). Dotted line was determined by linear regression analysis (slope = 62.25, R^2 = 0.44).

molecular characteristic to the trisaccharide antigen. Attained sensitivity and selectivity both contributed to the success of single-step "wash-free" measurement. A calibration plot of λ_{max} as a function of anti-A antibody concentration shows a detection limit of <10 μg/mL (Figure 3). This plot is based on the specific shift subtracted by nonspecific shift. Thus, a lower bound of error bar should simply exceed zero at the detection limit. Using a streptavidin-biotin reaction in diluted human blood, Wang et al

Table 1
Pearson correlation coefficients between assays

	TT (IgG)	SPR (Total)	SPR (IgG)
LSPR (Total)	0.70	0.80	0.78
LSPR (IgG)	0.66	0.80	0.79

The correlation coefficients were computed with the data from the common 41 serum samples.

obtained a detection limit of about 3 μg/mL.[13] We are convinced that our results are within a reasonable range using an antigen-antibody reaction.

In comparison with other methods, we observed at least moderately strong correlations among them (Table 1). A statistical interpretation of R-squares is that at most, 44% and 63% of variability of the results in LSPR were to be explained by TT and SPR, respectively (Figure 5). In other words, we should be cautious about considering other factors that influence the measurements. This is because such methods do not necessarily measure exactly the same events that LSPR measures. Particularly, TT is less quantitative, for which results are discrete values based on serial dilutions and visual observation. Moreover, SPR uses a flow-cell system, which means it detects a dynamic process of binding events, not a static process. These diferences would contribute to the decreased correlations or R–squares.

It is well known that human serum has several isotypes of antibody dominated by IgG and IgM, which was confirmed by the TT method here. We consider it in the case of our assay. We suppose that LSPR and SPR detect mostly the IgG-type antibody, which we presume from their similar responses even without the use of the secondary antibody. That secondary antibody was used to distinguish IgG and IgM. This is, to some extent, due to the higher K_d of IgM antibodies in a monovalent intereraction[18] between antigen-binding region and immobilized antigen than that of IgG. In our assay by LSPR or SPR, IgG and IgM competed against each other for the same targeting antigen. Our observation of results, however, is that the major responses are caused by the reaction of IgG, owing to its higher affinity to the antigen than IgM. Therefore, we conclude that LSPR could substitute for the function of SPR in measuring antibody titers and improve the operability in clinical practice because of their similar diagnostic characteristics in terms of the isotypes of antibody to be measured.

Two features of our method are worth mentioning with respect to the clinical diagnostics. First, our assay is simple, and a single-step operation is possible. Figure 4 reveals the equivalency of responses between "wash" and "wash-free" measurements. The near-zero intercept also indicates the competence of our technique to prevent nonspecific adsorption from serum contents. This is owing to the spatial characteristic of the LSPR biosensor as illustrated in the Graphical Abstract. Specifically, LSPR has a smaller sensing volume than SPR, which is appropriate to exclusively detect the surface binding events. In addition, we have optimized the sensing volume for detecting antibodies as reported previously.[15] We emphasize this property because none of the conventional methods is able to measure quantitatively with a single step. This observation would bring a huge benefit in clinical practice because the only required

procedure to get accurate diagnostic results is to put the test solution into a reaction well. This means a substantial reduction of total operational time to measure the concentration of antibodies. In addition, it could eliminate other laborious manual steps like washing wells, which can cause deviation in the responses obtained by many laboratory technicians in clinical practice. Furthermore, intermittent monitoring of specific markers in the sample could be easily conducted in a clinical setting using our method because the quality of each measurement well can be precisely controlled. For example, monitoring the change in the amount of anti-human blood group antigen antibodies is essential for prognosis after the ABO-unmatched transplant. The risk of adverse events in the case of ABO-incompatible living-liver transplantation would decrease significantly with timely monitoring and appropriate remedies. With the help of our methods, physicians will have better opportunities to more accurately follow up on patients' critical responses to the transplants than in the past.

Second, as our assay used microtiter plates, we are easily able to multiplex the measurement because the required sample is small and the operation is simple. In many situations, physicians are interested in a set of different antibodies or biomolecules to improve the performance of diagnosis of a patient's condition. For instance, multiplexed markers for autoimmune diseases or tumors are used and explored.[19-22]

Further intensive study is necessary to improve this assay. A major drawback to our demonstrated method is the use of reference wells, which is also a fundamental challenge in the development of label-free optical biosensors. This duplicates the operation to improve signal intensity. However, we hope to find a way to obtain accurate results even without reference wells. Moreover, this single-well measurement will provide a real-time measurement of molecular binding events, which enables us to understand the affinity and kinetics of that binding event similarly by the SPR method.

In conclusion, we have shown a single-step, label-free quantification of anti-A antibodies in human serum. Our method achieved a simple, efficient and reliable way to specifically detect antibodies in crude serum samples. These results point to the vast applicability of our LSPR method to measure the level of antibodies in the test solution by adopting various kinds of antigens immobilized on AuNPs. We believe that the LSPR method will have the potential to be routinely used as a rapid and cost-effective diagnostic method in the future.

Appendix A. Supplementary data

Supplementary data to this article can be found online at doi:10.1016/j.nano.2011.02.002.

References

1. Egawa H, Teramukai S, Haga H, Tanabe M, Fukushima M, Shimazu M. Present status of ABO-Incompatible living donor liver transplantation in Japan. Hepatology 2008;47:143-52.
2. Homola J, Yee SS, Gauglitz G. Surface plasmon resonance sensors: review. Sens Actuators B: Chem 2000;63:24-30.
3. Englebienne P, Van Hoonacker A, Verhas M. Surface plasmon resonance: principles, methods and applications in biomedical sciences. Spectrosc 2003;17:255-73.
4. Campbell CT, Kim G. SPR microscopy and its applications to high-throughput analyses of biomolecular binding events and their kinetics. Biomater 2007;28:2380-92.
5. Kimura S, Yurugi K, Segawa H, Kuroda J, Sato K, Nogawa M, et al. Rapid quantitation of immunoglobulin G antibodies specific for blood group antigens A and B by surface plasmon resonance. Transfusion 2005;45:56-62.
6. Yurugi K, Kimura S, Ashihara E, Tsuji H, Kawata A, Kamitsuji Y, et al. Rapid and accurate measurement of anti-A/B IgG antibody in ABO-unmatched living donor liver transplantation by surface plasmon resonance. Transfusion Med 2007;17:97-106.
7. Kobayashi T. Standardization of the assay method for anti-A/B antibody titers and its problems. Int Congress Series 2006;1292:3-7.
8. Anker JN, Hall WP, Lyandres O, Shah NC, Zhao J, Van Duyne RP, et al. Biosensing with plasmonic nanosensors. Nat Mater 2008; 7:442-53.
9. Nath N, Chilkoti AA. Colorimetric Gold nanoparticle sensor to interrogate biomolecular interactions in real time on a surface. Anal Chem 2002;74:504-9.
10. Englebienne P. Use of colloidal gold surface plasmon resonance peak shift to infer affinity constants from the interactions between protein antigens and antibodies specific for single or multiple epitopes. Analyst 1998;123:1599-603.
11. Haes AJ, Chang L, Klein WL, Van Duyne RP. Detection of a biomarker for Alzheimer's disease from synthetic and clinical samples using a nanoscale optical biosensor. J Am Chem Soc 2005;127:2264-71.
12. Mayer KM, Lee S, Liao H, Rostro BC, Fuentes A, Scully PT, et al. A label-free immunoassay based upon localized surface plasmon resonance of gold nanorods. ACS Nano 2008;2:687-92.
13. Wang Y, Qian W, Tan Y, Ding S. A label-free biosensor based on gold nanoshell monolayers for monitoring biomolecular interactions in diluted whole blood. Biosens Bioelectron 2008;23:1166-70.
14. Endo T, Kerman K, Nagatani N, Takamura Y, Tamiya E. Label-free detection of peptide nucleic acid-DNA hybridization using localized surface plasmon resonance based optical biosensor. Anal Chem 2005;77:6976-84.
15. Yamamichi J, Iida M, Ojima T, Handa Y, Yamada T, Kuroda R, et al. The mesoscopic effect on label-free biosensors based on localized surface plasmon resonance of immobilized colloidal gold. Sens Actuators B: Chem 2009;143:349-56.
16. Kelly KL, Coronado E, Zhao LL, Schatz GC. The optical properties of metal nanoparticles: the influence of size, shape, and dielectric environment. J Phys Chem B 2003;107:668-77.
17. Miller MM, Lazarides AA. Sensitivity of metal nanoparticle plasmon resonance band position to the dielectric environment as observed in scattering. J Opt A: Pure Appl Opt 2006;8:S239-49.
18. Strandh M, Ohlin M, Borrebaeck CAK, Ohlson S. New approach to steroid separation based on a low affinity IgM antibody. J Immunol Methods 1998;214:73-9.
19. Döner T, Hansen A. Autoantibodies in normals - the value of predicting rheumatoid arthritis. Arthritis Res Ther 2004;6:282-4.
20. Hanly JG, Thompson K, McCurdy G, Fougere L, Theriault C, Wilton K. Measurement of autoantibodies using multiplex methodology in patients with systemic lupus erythematosus. J Immunol Methods 2010;352: 147-52.
21. Binder S. Autoantibody Detection Using Multiplex Technologies. Lupus 2006;15:412-21.
22. Vojdani A. Antibodies as predictors of complex autoimmune diseases and cancer. Int J Immunopathol Pharmacol 2008;21:553-66.

Oncogene (2011) 30, 2789–2797

www.nature.com/onc

ORIGINAL ARTICLE

Combined effects of novel heat shock protein 90 inhibitor NVP-AUY922 and nilotinib in a random mutagenesis screen

T Tauchi[1], S Okabe[1], E Ashihara[2], S Kimura[3], T Maekawa[4] and K Ohyashiki[1]

[1]*First Department of Internal Medicine, Tokyo Medical University, Tokyo, Japan;* [2]*Department of Molecular Cell Physiology, Kyoto Prefectural University of Medicine, Kyoto, Japan;* [3]*Division of Hematology, Respiratory Medicine and Oncology, Department of Internal Medicine, Faculty of Medicine, Saga University, Saga, Japan and* [4]*Department of Transfusion Medicine and Cell Therapy, Faculty of Medicine, Kyoto University, Kyoto, Japan*

To overcome imatinib resistance, more potent ABL tyrosine kinase inhibitors (TKIs), such as nilotinib and dasatinib have been developed, with demonstrable preclinical activity against most imatinib-resistant BCR–ABL kinase domain mutations, with the exception of T315I. However, imatinib-resistant patients already harboring mutations have a higher likelihood of developing further mutations under the selective pressure of potent ABL TKIs. NVP-AUY922 (Novartis) is a novel 4,5-diaryloxazole adenosine triphosphate-binding site heat shock protein 90 (HSP90) inhibitor, which has been shown to inhibit the chaperone function of HSP90 and deplete the levels of HSP90 client protein including BCR–ABL. In this study, we investigated the combined effects of AUY922 and nilotinib on random mutagenesis for BCR–ABL mutation (Blood, 109; 5011, 2007). Compared with single agents, combination with AUY922 and nilotinib was more effective at reducing the outgrowth of resistant cell clones. No outgrowth was observed in the presence of 2 μM of nilotinib and 20 nM of AUY922. The observed data from the isobologram indicated the synergistic effect of simultaneous exposure to AUY922 and nilotinib even in BaF3 cells expressing BCR–ABL mutants including T315I. *In vivo* studies also demonstrated that the combination of AUY922 and nilotinib prolonged the survival of mice transplanted with mixture of BaF3 cells expressing wild-type BCR–ABL and mutant forms. Taken together, this study shows that the combination of AUY922 and nilotinib exhibits a desirable therapeutic index that can reduce the *in vivo* growth of mutant forms of BCR–ABL-expressing cells.

Oncogene (2011) **30,** 2789–2797; doi:10.1038/onc.2011.3; published online 31 January 2011

Keywords: BCR–ABL; tyrosine kinase inhibitor; nilotinib; HSP90; T315I

Correspondence: Dr T Tauchi, First Department of Internal Medicine, Tokyo Medical University, 6-7-1 Nishishinjuku, Shinjuku-ku, Tokyo 160-0023, Japan.
E-mail: tauchi@tokyo-med.ac.jp
Received 10 February 2010; revised 15 November 2010; accepted 1 January 2011; published online 31 January 2011

Introduction

Resistance to the ABL tyrosine kinase inhibitor (TKI), imatinib, in Ph-positive leukemia is often caused by selection of mutations in BCR–ABL kinase domain altering residues that are directly or indirectly critical for imatinib binding (O'Hare *et al.*, 2007). To overcome imatinib resistance, more potent ABL TKIs, such as nilotinib and dasatinib have been developed, with demonstrable preclinical activity against most imatinib-resistant BCR–ABL kinase domain mutations, with the exception of T315I (Shah *et al.*, 2004; Weisberg *et al.*, 2005). The T315I is the single most frequent mutation that outgrows and leads to relapse during nilotinib and imatinib-treatment (Jabbour *et al.*, 2008). Other mutations, however, are found to have emerged at the time of relapse in ABL TKI-resistant patients (Branford *et al.*, 2009). F359V and the P-loop mutants Y253H and E255K/V are associated with relapse to nilotinib, and F317A/L and V299L are found in dasatinib-resistant patients (Branford *et al.*, 2009). Imatinib-resistant patients already harboring mutations have a higher likelihood of developing further mutations under the selective pressure of ABL TKIs (Garg *et al.*, 2009). The challenge for development of an effective Ph-positive leukemia therapy is therefore to develop an alternative treatment strategy that does not rely solely on kinase domain inhibition but rather results in degradation of the offending BCR–ABL protein regardless of its mutation status.

NVP-AUY922 is a novel 4,5-diaryloxazole adenosine triphosphate-binding site heat shock protein 90 (HSP90) inhibitor, which has been shown to inhibit the chaperone function of HSP90 and deplete the levels of HSP90 client protein (for example, ErbB2, Akt, Raf and Bcr–Abl) (Brough *et al.*, 2008; Eccles *et al.*, 2008; Stuhmer *et al.*, 2008). Combining AUY922 with ABL kinase inhibitors may provide several advantages, such as enhanced efficacy and reducing the potential emergence of new resistant mutations. In this study, we performed a comprehensive drug combination experiment using a broader range of concentrations for AUY922 and nilotinib or imatinib. Compared with single agents, combination with AUY922 and nilotinib was more effective at reducing the outgrowth of resistant cell clones. At the highest concentration of nilotinib, the

mutation spectrum narrowed to T315I and E344V by direct sequencing, whereas, at intermediate concentration of AUY922, the resistant clone was recovered by wild-type (WT) BCR–ABL only. The observed data from the isobologram indicated the synergistic effect of simultaneous exposure to AUY922 and nilotinib even in BaF3 cells expressing BCR–ABL mutants including T315I. *In vivo* studies also demonstrated that the combination of AUY922 and nilotinib prolonged the survival of mice transplanted with mixture of BaF3 cells expressing WT BCR–ABL and mutant forms. Taken together, this study shows that the combination of AUY922 and nilotinib exhibits a desirable therapeutic index that can reduce the *in vivo* growth of mutant forms of BCR–ABL-expressing cells.

Results

AUY922 in combination with nilotinib or imatinib completely suppresses outgrowth of resistant clones by random mutagenesis screen

To assess whether combinations of ABL kinase inhibitors offer an advantage over AUY922 alone, we carried out a random mutagenesis screens with combinations of AUY922 and imatinib or nilotinib (Ray *et al.*, 2007). This approach uses a DNA repair-deficient *Escherichia coli* strain to produce random mutagenesis of a BCR–ABL retroviral plasmid, infection of BaF3 cells and selection for BaF3 clones conferring varying degree of drug resistance (Ray *et al.*, 2007). Profiling of AUY922 as a single agent revealed a concentration-dependent reduction of colonies (Figure 1). Sequencing revealed only WT BCR–ABL in AUY922-resistant clones, with the lowest concentration of AUY922 and 500 nM of imatinib (Figure 1). Sequencing of nilotinib-resistant clones with the highest concentration (2 μM) revealed T315I and E344V (Figure 1). We then performed a comprehensive drug combination using a broader range of concentrations of AUY922 and nilotinib or imatinib. Compared with single agent, combinations with AUY922 and nilotinib or AUY922 and imatinib were more effective at reducing the outgrowth of resistant clones. No outgrowth was observed in the presence of 2 μM of nilotinib and 20 nM of AUY922 (Figure 1).

Combined effects of AUY922 and nilotinib in mutant forms of BCR–ABL-expressing cells

We used the isobologram method to determine whether the combined effects of AUY922 and nilotinib are additive or synergistic in mutant forms of BCR–ABL-expressing BaF3 cells. Figure 2a showed the dose-response curve for AUY922 and nilotinib in WT-p210 BCR–ABL-expressing BaF3 cells. The isobologram was generated on the dose-response curve. The observed data from the isobologram indicated the synergistic effect on simultaneous exposure to AUY922 and nilotinib in WT BCR–ABL-expressing BaF3 cells (Figure 2a). M351T is a sensitive mutation to nilotinib, on the other hand, E255K is an insensitive mutation to

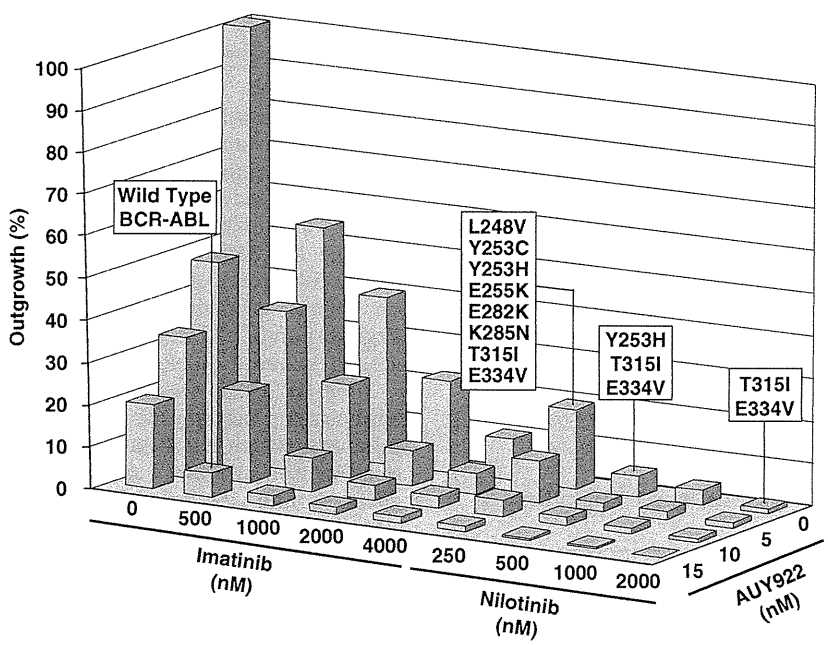

Figure 1 AUY922 in combination with nilotinib or imatinib completely suppresses outgrowth of resistant clones. The approach uses a DNA repair-deficient *Escherichia coli* strain to produce random mutagenesis of a BCR–ABL retroviral plasmid, infection of BaF3 cells, and selection for BaF3 clones conferring varying degree of drug resistance using methods previously described (Azam *et al.*, 2003). BaF3 cells expressing the random mutagenesis of BCR–ABL were kindly provided by Dr James D Griffin (Dana-Farber Cancer Institute) (Ray *et al.*, 2007). BaF3 cells expressing the random mutagenesis of a BCR–ABL were cultured with graded concentrations of AUY922 alone and in combination with imatinib or nilotinib. Bars represent the percentage of wells from which drug-resistant clones were recovered. Similar results were obtained in three independent experiments.

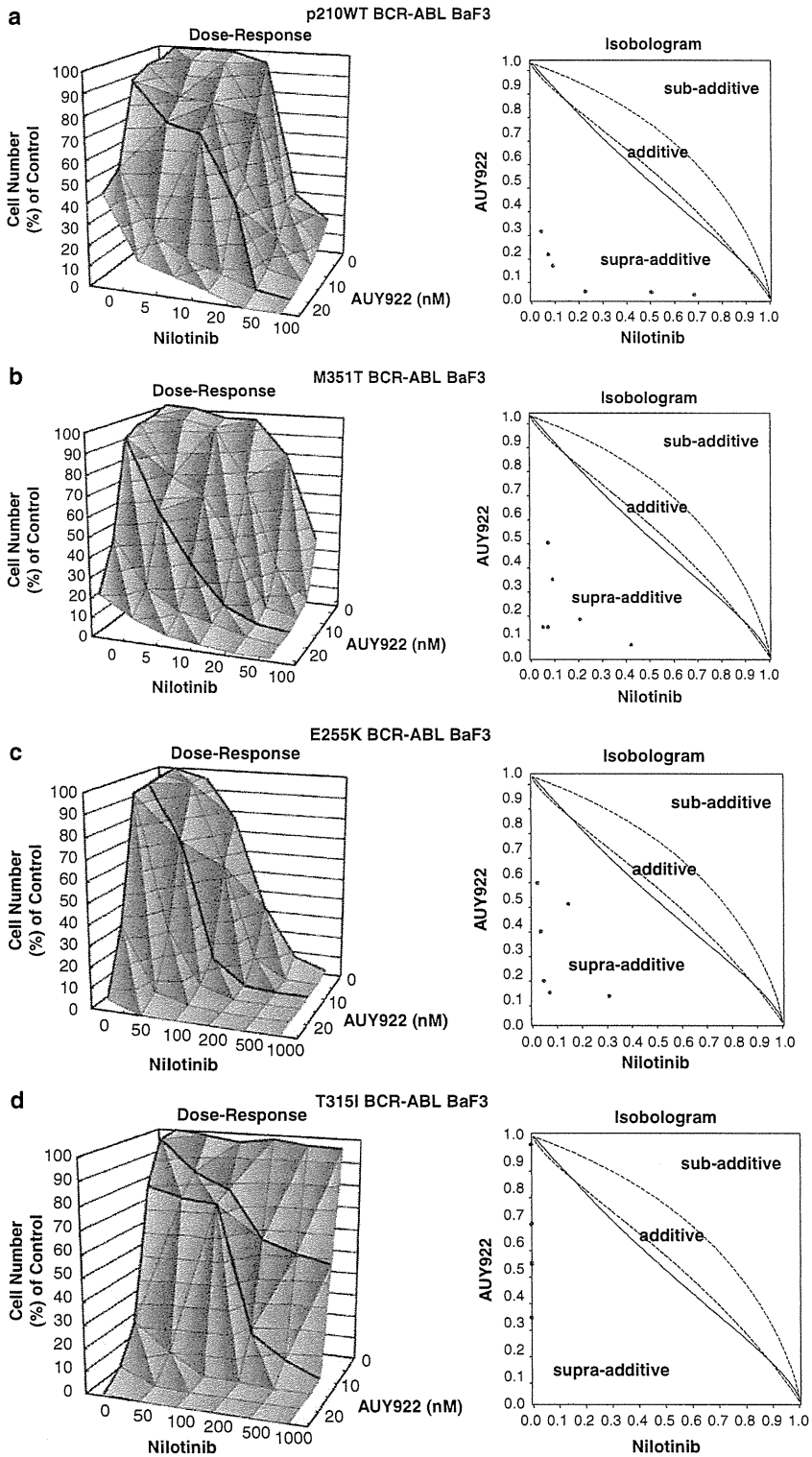

Figure 2 Combined effects of AUY922 and nilotinib in mutant forms of BCR–ABL-expressing cells. The theoretical basis of isobologram method and the procedure for making isobolograms have previously been described in detail (Kano *et al.*, 2001). The dose-response curves and generated isobologram for AUY922 and nilotinib were shown in Figure **a** (WT p210 BCR–ABL), **b** (M351T BCR–ABL), **c** (E255K BCR–ABL) and **d** (T315I BCR–ABL). The observed data from the isobologram indicated the synergistic effect of simultaneous exposure to AUY922 and nilotinib even in BaF3 cells expressing BCR–ABL mutants including T315I. Similar results were obtained in three independent experiments.

nilotinib. The isobolograms show the combination with AUY922 and nilotinib has the synergistic effect on both mutation (Figures 2b and c). In constant, T315I BaF3 cells were resistant to nilotinib up to levels as high as 2 μM, however, the treatment with AUY922 and nilotinib showed the synergistic effect in T315I BCR–ABL BaF3 cells (Figure 2d). Next, we determined the colony growth of WT BCR–ABL BaF3 cells and WT BCR–ABL-expressing primary chronic myeloid leukemia (CML) mononuclear cells (Figure 3a). Co-treatment with AUY922 and nilotinib caused significantly more inhibition of colony growth than treatment of either agent alone in WT BCR–ABL BaF3 cells and primary CML cells (Figure 3a). Further, we examined the colony growth of T315I BaF3 cells and T315I-expressing primary cells (Figure 3b). Co-treatment with AUY922 and nilotinib caused significantly more inhibition of colony growth than treatment of either agent alone in T315I BaF3 cells and T315I-expressing primary leukemia cells (Figure 3b). WT BCR–ABL BaF3 cells and

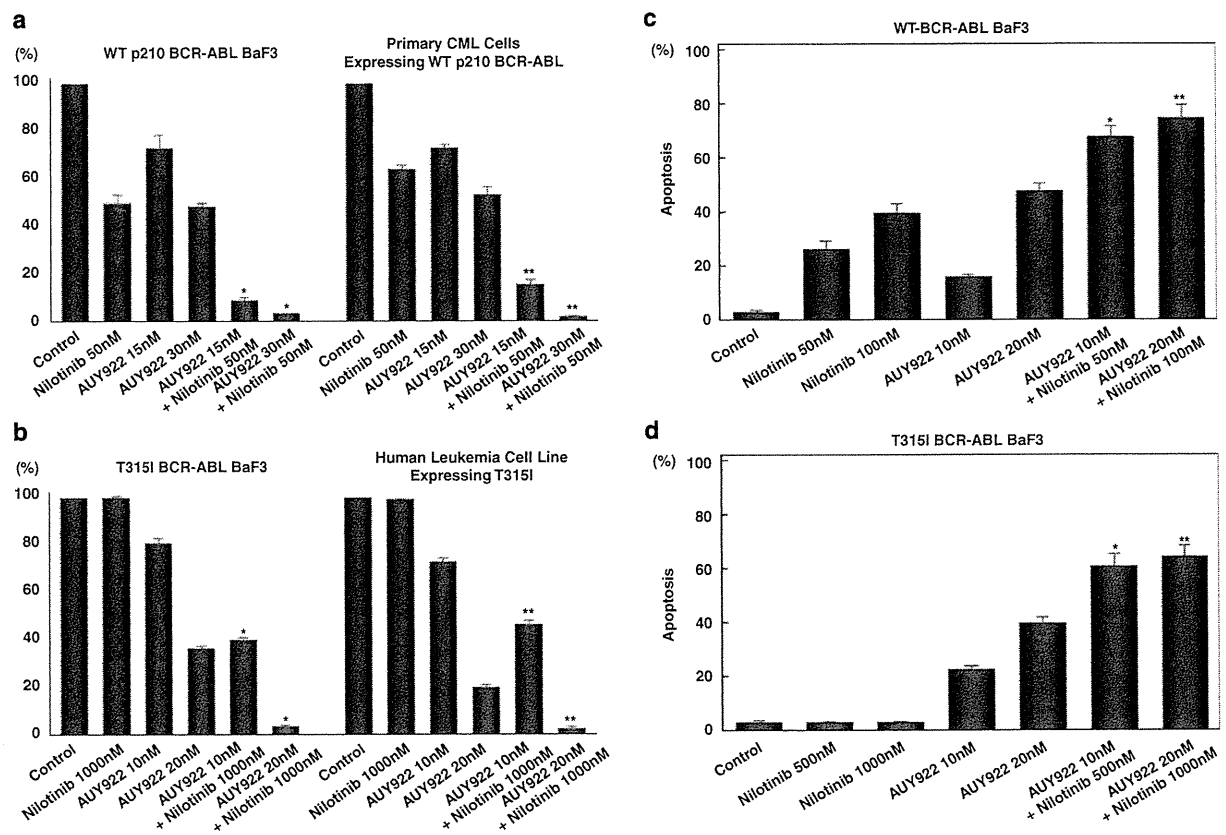

Figure 3 Co-treatment of AUY922 and nilotinib suppresses colony formation of in WT BCR–ABL and T315I BCR–ABL-expressing cells, and enhances the induction of apoptosis. (**a**) WT BCR–ABL BaF3 cells and WT BCR–ABL-expressing primary CML mononuclear cells were grown in methylcellulose containing the indicated concentrations of AUY922 and nilotinib. Colony counts were assessed on each individual sample at least twice, and results are presented as average ± s.d. for colonies counted from triplicate plates under each condition. WT BCR–ABL BaF3 cells; nilotinib 50 nM: 49.1 ± 3.5%, AUY922 15 nM: 73.5 ± 5.5%, AUY922 30 nM: 48.4 ± 1.4%, AUY922 15 nM + nilotinib 50 nM: 9.4 ± 0.3%, AUY922 30 nM + nilotinib 50 nM: 3.5 ± 0.1%, respectively. $*P<0.01$ compared with nilotinib 50 nM-treatment. WT BCR–ABL-expressing primary CML mononuclear cells; nilotinib 50 nM: 64.3 ± 1.9%, AUY922 15 nM: 73.3 ± 1.3%, AUY922 30 nM: 53.2 ± 3.1%, AUY922 15 nM + nilotinib 50 nM: 16.1 ± 1.8%, AUY922 30 nM + nilotinib 50 nM: 1.8 ± 0.1%, respectively. $**P<0.01$ compared with nilotinib 50 nM-treatment. (**b**) T315I BaF3 cells and T315I-expressing primary cells were grown in methylcellulose containing the indicated concentrations of AUY922 and nilotinib. Colony counts were assessed on each individual sample at least twice, and results are presented as average ± s.d. for colonies counted from triplicate plates under each condition. T315I BaF3 cells; nilotinib 1000 nM: 99.1 ± 0.8%, AUY922 10 nM: 81.5 ± 1.9%, AUY922 20 nM: 37.2 ± 0.8%, AUY922 10 nM + nilotinib 1000 nM: 40.2 ± 0.9%, AUY922 20 nM + nilotinib 1000 nM: 3.8 ± 0.2%, respectively. $*P<0.01$ compared with nilotinib 1000 nM-treatment. T315I-expressing primary cells; nilotinib 1000 nM: 99.2 ± 0.1%, AUY922 10 nM: 73.5 ± 1.3%, AUY922 20 nM: 20.1 ± 0.9%, AUY922 10 nM + nilotinib 1000 nM: 46.9 ± 1.4%, AUY922 20 nM + nilotinib 1000 nM: 2.1 ± 0.4%, respectively. $**P<0.01$ compared with nilotinib 1000 nM-treatment. WT BCR–ABL BaF3 cells (**c**) and T315I BaF3 cells (**d**) were cultured with the indicated concentrations of AUY922 and nilotinib for 72 h, after which the percentage of apoptotic cells was determined by annexin-V. (**c**) WT BCR–ABL BaF3 cells; control: 3.3 ± 0.8%, nilotinib 50 nM: 25.8 ± 2.2%, nilotinib 100 nM: 39.6 ± 2.7%: AUY922 10 nM: 14.3 ± 0.9%, AUY922 20 nM: 43.2 ± 3.2%, AUY922 10 nM + nilotinib 50 nM: 67.8 ± 3.2%, AUY922 20 nM + nilotinib 100 nM: 74.5 ± 4.4%, respectively. $*P<0.01$ compared with nilotinib 50 nM-treatment. $**P<0.01$ compared with nilotinib 100 nM-treatment. (**d**) T315I BaF3 cells; control: 2.1 ± 0.5%, nilotinib 500 nM: 2.0 ± 0.1%, nilotinib 1000 nM: 2.1 ± 0.1%, AUY922 10 nM: 22.9 ± 0.8%, AUY922 20 nM: 39.6 ± 1.9%, AUY922 10 nM + nilotinib 500 nM: 60.2 ± 3.9%, AUY922 20 nM + nilotinib 1000 nM: 62.4 ± 3.8%, respectively. $*P<0.01$ compared with nilotinib 500 nM-treatment. $**P<0.01$ compared with nilotinib 1000 nM-treatment.

T315I BaF3 cells were cultured with the indicated concentrations of AUY922 and nilotinib for 72 h, after which the percentage of apoptotic cells was determined by annexin-V (Figures 3c and d). When 10 nM of AUY922 was combined with nilotinib in WT BCR–ABL BaF3 cells, the increase in apoptotic cells was virtually complete for nilotinib concentrations higher than 1 μM (Figure 3c). Treatment with 1 μM of nilotinib had no effect on T315I BaF3 cells, however, co-treatment of AUY922 and nilotinib also enhanced the induction of apoptosis in T315I BaF3 cells (Figure 3d). Together, these findings indicate that combination of minimally toxic concentrations of AUY922 and nilotinib is effective in inducing apoptosis in both WT BCR–ABL-expressing cells and T315I BCR–ABL-expressing cells.

AUY922 induces degradation of WT and mutant forms of BCR–ABL proteins

Previous studies have shown that the HSP90 inhibitors geldanamycine and 17-AAG disrupt HSP90 function and induce BCR–ABL degradation (Gorre *et al.*, 2002). To determine whether AUY922 can similarly cause the degradation of BCR–ABL proteins, WT, T315I, E255K or M351T BCR–ABL-expressing BaF3 cells were exposed to varying concentrations of AUY922 for 24 h (Figures 4a and b). Immunoblot analysis revealed that AUY922 caused BCR–ABL protein levels to decrease significantly in WT BCR–ABL-expressing BaF3 cells at a dose of 50 nM, as expected (Figure 4a). Mutant forms of BCR–ABL proteins were also degraded at a lower concentration of AUY922 (Figures 4a and b). These results suggest that AUY922 may have greater potency against mutant forms of BCR–ABL proteins compared with WT.

The mechanism of the synergism between AUY922 and nilotinib in T315I BCR–ABL BaF3 cells

We next conducted the experiments to further evaluate the mechanism of the synergism between AUY922 and nilotinib in T315I BCR–ABL BaF3 cells. Besides the ABL kinases, the receptor tyrosine kinase DDR1 and the oxidoreductase NQO2 are target molecules for nilotinib (Bantscheff *et al.*, 2007; Rix *et al.*, 2007). T315I BaF3 cells were cultured with the indicated concentrations of nilotinib for 24 h, the cell lysates were

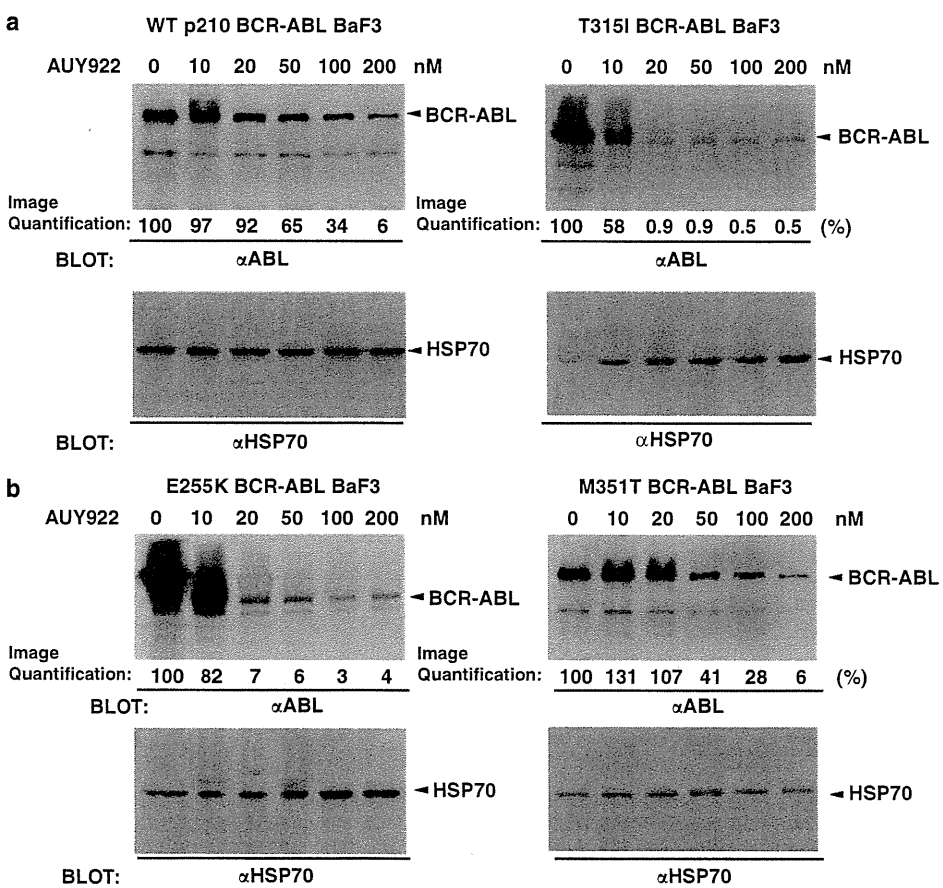

Figure 4 AUY922 induces degradation of WT and mutant forms of BCR–ABL proteins. (**a**) WT or T315I BCR–ABL-expressing BaF3 cells were exposed to varying concentrations of AUY922 for 24 h. The cell lysates were immunobloted with anti-ABL Ab or anti-HSP70 Ab. (**b**) E255K, or M351T BCR–ABL-expressing BaF3 cells were exposed to varying concentrations of AUY922 for 24 h. The cell lysates were immunobloted with anti-ABL Ab or anti-HSP70 Ab.

immunoprecipitated with anti-DDR1 antibody (Ab) and then immunoblotted with anti-phosphotyrosine mAb (PY20) or anti-DDR1 Ab (Figure 5a). Higher concentrations of nilotinib abolished DDR1 autophosphorylation (Figure 5a). To assess the functional importance of DDR1 and NQO2, we used RNA interference to determine whether reduction in DDR1 and NQO2 affect the proliferation of T315I BaF3 cells after the treatment of AUY922. T315I BaF3 cells were transfected with control small interfering RNA (siRNA) or *DDR1* siRNA or *NQO2* siRNA; then the DDR1 and NQO2 expression was analyzed by immunoblotting after 48 h (Figure 5b). At 48 h after transfection, T315I BCR–ABL BaF3 cells were treated with indicated concentration of AUY922 for 48 h, and viable cells were counted (Figure 5c). In the presence of *DDR1* siRNA, T315I BCR–ABL BaF3 cells increased antiproliferative activity with AUY922 (at 5 or 10 nM) (Figure 5c). When AUY922 was treated in the presence of *NQO2* siRNA, antiproliferative activity of T315I BCR–ABL was not observed (Figure 5c). These results showed that inhibition of DDR1 can have an important role in the synergism between AUY922 and nilotinib.

Further, we examined the phosphorylation of T315I BCR–ABL after treatment of AUY922 and nilotinib. T315I BCR–ABL BaF3 cells were cultured with indicated concentrations of AUY922 and nilotinib for 24 h. The cell lysates were immunoblotted with anti-phosho-ABL Ab or anti-ABL Ab (Figure 5d). Co-treatment with AUY922 and nilotinib partially decreased auto-phosphorylation of T315I BCR–ABL (Figure 5d).

Co-treatment of AUY922 and nilotinib prolong the survival in mice model of BCR–ABL mutant-induced leukemia

We investigate the *in vivo* efficacy of AUY922 and nilotinib (Figure 6). Twelve-week-old nude mice were injected with 5×10^5 cells of mixture of BaF3 cells expressing WT BCR–ABL and mutant forms of BCR–ABL (M244V, G250E, Q252H, Y253F, T315A, T315I, F317L, F317V, M351T and H396P). At 24-h injection of the leukemia cells, these mice were treated with either vehicle or AUY922 (50 mg/kg intraperitoneal (i.p.); two times per week) or nilotinib (30 mg/kg; q.d.) or AUY922 (50 mg/kg i.p.; two times per week) + nilotinib

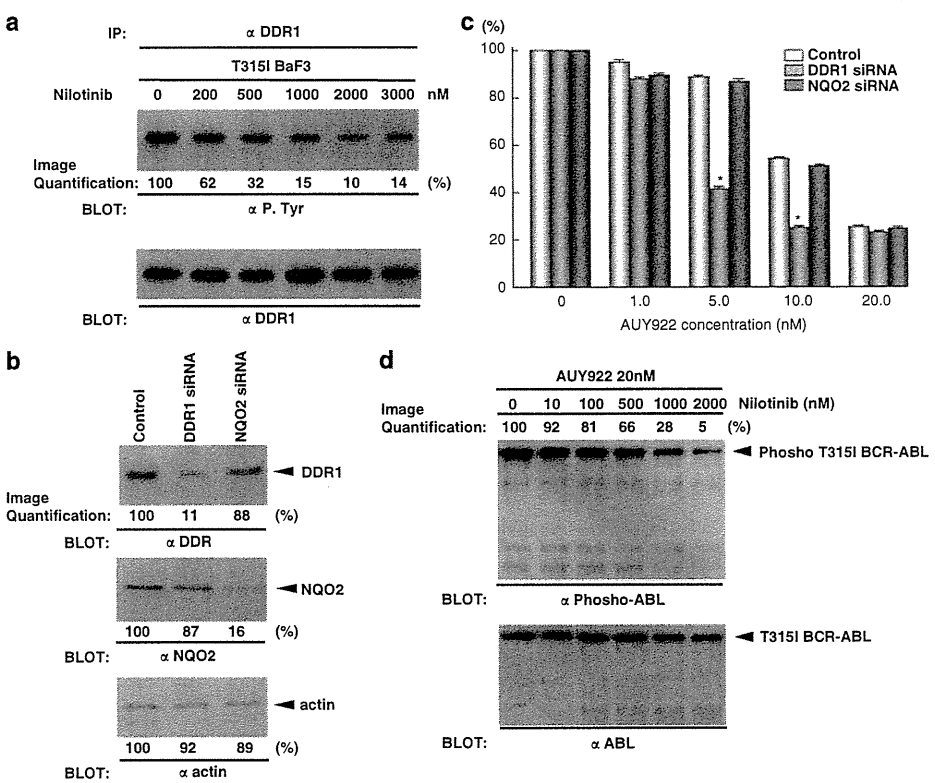

Figure 5 The mechanism of the synergism between AUY922 and nilotinib in T315I BCR–ABL BaF3 cells. (**a**) T315I BaF3 cells were cultured with the indicated concentrations of nilotinib for 24 h, the cell lysates were immunoprecipitated with anti-DDR1 Ab and then immunoblotted with anti-phosphotyrosine mAb or anti-DDR1 Ab. (**b**) T315I BaF3 cells were transfected with control siRNA or *DDR1* siRNA or *NQO2* siRNA; then the DDR1 and NQO2 expression was analyzed by immunoblotting after 48 h. (**c**) At 48 h after transfection, T315I BCR–ABL BaF3 cells were treated with indicated concentration of AUY922 for 48 h, and viable cells were counted by using Vi-cell XR automated cell viability analyzer (Beckman Coulter). The mean number of viable cells at different concentration of drug was normalized to the mean number of viable cells in the no-drug samples. $^*P<0.01$ compared with contro siRNA-treatment. Similar results were obtained in each of three independent experiments. (**d**) T315I BCR–ABL BaF3 cells were cultured with indicated concentrations of AUY922 and nilotinib for 24 h. The cell lysates were immunoblotted with anti-phosho-ABL Ab or anti-ABL Ab.

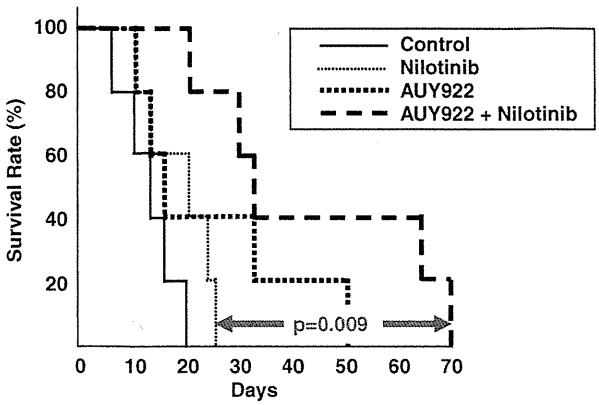

Figure 6 Co-treatment of AUY922 and nilotinib prolong the survival in mice model of BCR–ABL mutant-induced leukemia. Nude mice were injected with 5×10^5 cells of mixture of BaF3 cells expressing WT BCR–ABL and mutant forms of BCR–ABL (M244V, G250E, Q252H, Y253F, T315A, T315I, F317L, F317V, M351T and H396P). At 24-h injection of the leukemia cells, these mice were treated with either vehicle or AUY922 (50 mg/kg i.p.; two times per week) or nilotinib (30 mg/kg; q.d.) or AUY922 (50 mg/kg i.p.; two times per week) + nilotinib (30 mg/kg; q.d.).

(30 mg/kg; q.d.). The vehicle or nilotinib-treated mice died of a condition resembling acute leukemia by 28 days; the combination of AUY922 + nilotinib-treated mice survived more than 60 days, significantly improved the survival ($P = 0.009$) compared with nilotinib-treated mice (Figure 6).

Discussion

Second-generation TKIs have demonstrated increased inhibitory potency against BCR–ABL tyrosine kinase and have shown efficacy in treating patients with number of the BCR–ABL kinase domain mutations that develop on imatinib (Kantarjian *et al.*, 2006, 2007, 2009; Ottmann *et al.*, 2007). Despite the significant clinical activity demonstrated in clinical trials, a number of patients do not show durable response (Garg *et al.*, 2009). One reason for the lack of durable response could be explained by the emergence of new kinase domain mutations as patients are exposed to sequential TKIs (Branford *et al.*, 2009; Garg *et al.*, 2009). The challenge for development of an effective Ph-positive leukemia therapy is therefore to develop an alternative treatment strategy that does not rely solely on kinase domain inhibition but rather results in degradation of the offending BCR–ABL protein regardless of its mutation status.

AUY922 is a most potent resorcinylic isoxazole amide HSP90 inhibitor, which binds to the adenosine triphosphate-binding pocket of HSP90 (Brough *et al.*, 2008). AUY922 has excellent cellular potency against a panel of tumor cell lines (Brough *et al.*, 2008; Eccles *et al.*, 2008; Stuhmer *et al.*, 2008). In addition, optimization of pharmacokinetic properties led to robust therapeutic responses in a wide variety of human tumor xenografts tightly linked to high intratumor concentrations of compound and phamacodynamic response (Eccles *et al.*, 2008). The promising preclinical data obtained with AUY922 supported the initiation of clinical phase I trials in patients with solid tumors.

In this study, we investigated a comprehensive drug combination experiment using a broader range of concentrations for AUY922 and nilotinib or imatinib by saturation mutagenesis screen (Figure 1). AUY922 controlled the outgrowth of WT BCR–ABL, and mutated forms of BCR–ABL associated with imatinib or nilotinib resistance (Figure 1). When AUY922 was included with imatinib or nilotinib, outgrowth of resistant subclones were significantly reduced (Figure 1). Although further pharmacokinetic analysis of AUY922 will be necessary, it is remarkable that even the lowest dose of AUY922 tested in combination with clinically relevant concentrations of nilotinib completely suppressed the emergence of resistant clone.

The T315I BCR–ABL mutation is emerging as a common mechanism of failure to second line ABL TKIs. Thus, even in advanced phase of CML, BCR–ABL remains the critical therapeutic target. So far, reports of successful salvage therapy for CML patients who acquire the T315I BCR–ABL mutation are limited to small clinical trials. The isobologram analysis indicated the synergistic effect of simultaneous exposure to AUY922 and nilotinib even in BaF3 cells expressing BCR–ABL mutants including T315I (Figure 2). Further, combination of AUY922 and nilotinib is also effective in inducing apoptosis in both WT BCR–ABL-expressing cells and T315I BCR–ABL-expressing cells (Figures 3c and d). These results indicate that co-treatment with AUY922 sensitizes T315I BCR–ABL-expressing cells to clinically achievable trough levels of nilotinib. However, the structural basis for how co-treatment with AUY922 leads to enhanced activity of nilotinib against the gatekeeper T315I BCR–ABL mutant is entirely unclear. It is possible that nilotinib may collaborate with AUY922 in significantly inhibiting the off-target tyrosine kinase besides BCR–ABL. DDR1 is thought to transducer signals to NFκB pathway (Matsuyama *et al.*, 2004). Higher concentrations of nilotinib abolished DDR1 phosphorylation (Figure 5a). Further, down regulation of *DDR1* by siRNA increased antiproliferative activity in AUY922-treated T3151 BCR–ABL BaF3 cells (Figure 5c). Our results clearly show that DDR1 may contribute at least in part to the synergism between AUY922 and nilotinib. Alternative possibility is that AUY922-mediated inhibition of HSP90 chaperon function for BCR–ABL affects the conformational change of BCR–ABL that allows higher concentrations of nilotinib to interact with T315I BCR–ABL. Co-treatment with AUY922 and nilotinib partially decreased autophosphorylation of T315I BCR–ABL (Figure 5d). In this regard, it is interesting to test whether AUY922 might influence the conformational dynamics of the adenosine triphosphate-binding site of

the 'gatekeeper' mutant, T315I BCR–ABL. Further studies are required to resolve these mechanisms.

The simultaneous use of AUY922 and nilotinib in chronic phase CML patients might prevent the development of nilotinib-resistant clones and inhibit growth of highly proliferative leukemia cells through inhibition of kinase activity, thereby providing a rationale for combination strategy. In a survival mouse model using BaF3 cells expressing WT BCR–ABL and mutant forms of BCR–ABL (M244V, G250E, Q252H, Y253F, T315A, T315I, F317L, F317V, M351T and H396P), co-treatments with AUY922 and nilotinib significantly improved the survival ($P = 0.009$) (Figure 6). The results from these studies suggest that combined use of AUY922 and nilotinib would be a viable strategy for preventing emergence of resistant clones in clinic.

In summary, our preclinical results indicate that AUY922 has potential as an important option for controlling resistance in CML. The combined results of cell-based and *in vivo* studies suggest that AUY922 exhibits sufficient activity against mutants form of BCR–ABL to warrant consideration for combined use with ABL TKIs. Although several HSP90 inhibitors have now entered clinical evaluation, it is expected that through new formulations of AUY922, orally administrable, it will be more favorably modulate the schedule for CML patients.

Materials and methods

Antibodies and reagents
Anti-ABL Ab (24-11), anti-HSP70 Ab, anti-DDR1 Ab and anti-NQO2 Ab were purchased from Santa Cruz Biotechnology, Inc. (Santa Cruz, CA, USA). Anti-phosphotyrosine mAb (PY20) was purchased from Becton Dickinson and Company (Franklin Lakes, NJ, USA). Anti-phospho-ABL Ab was obtained from Cell Signaling (Beverly, MA, USA). AUY922, nilotinib and imatinib were kindly provided by Novartis Pharma AG (Basel, Switzerland).

Cells and cell culture
The approach uses a DNA repair-deficient *E. coli* strain to produce random mutagenesis of a BCR–ABL retroviral plasmid, infection of BaF3 cells, and selection for BaF3 clones conferring varying degree of drug resistance. BaF3 cells expressing the random mutagenesis of BCR–ABL were kindly provided by Dr James D Griffin (Dana-Farber Cancer Institute, Boston, MA, USA) (Ray *et al.*, 2007). BaF3 cells expressing WT BCR–ABL and mutant forms of BCR–ABL (M244V, G250E, Q252H, Y253F, T315A, T315I, F317L, F317V, M351T and H396P) were described previously (Deguchi *et al.*, 2008). These cell lines were cultured in RPMI1640 (Life Technology, Inc., Carlsbad, CA, USA) supplemented with 10% fetal calf serum (Hyclone Laboratories, Logan, UT, USA).

The isobologram method
The theoretical basis of isobologram method and the procedure for making isobolograms have previously been described in detail (Kano *et al.*, 2001). Cells were suspended to a final concentration of 1×10^5 cells/ml in fresh medium, plated in 24-well dishes and incubated with AUY922 or imatinib or nilotinib or in combination at 37 °C for 72 h. The number of cells in each well was counted by flow cytometry, and the cell numbers were normalized by dividing the number of cells (Nunoda *et al.*, 2007).

Apoptosis assay
The cells were treated with the indicated concentration of AUY922 and/or nilotinib for 48 h. Annexin V/propidium iodide apoptosis assay was performed according to the manufacturer's protocol (Becton Dickinson and Company). The cells were gently mixed and immediately analyzed by flow cytometry.

Immunoblotting
Immunoblotting was performed as described previously (Tauchi *et al.*, 1994).

siRNA experiments
siRNA oligonucleotides for murine *DDR1* and *NQO2* were purchased from Santa Cruz Biotechnology, Inc., and resuspended in RNase-free H2O at 20 μM. siRNA (1.25 μM) was added to prechilled 0.4 cm-gap electroporation cuvetts (Bio-Rad, Hercules, CA, USA). T315I BaF3 cells (5×10^6) were washed twice in serum-free media and resuspended to 5×10^6 cells per 250 μl of cold, serum-free RPMI 1640. Cells were added to the cuvetts, mixed, and mixed on ice for 5 min. Cells were then pulsed once at 250 mV, 960 μF and 200 ohms by using a Bio-Rad electroporator. At 48 h after electroporation, protein knockdown was determined by immunoblotting, and cells were treated with the indicated concentration of dasatinib or imatinib for 48 h, viable cells were counted by using a Vi-cell XR automated cell viability analyzer (Beckman Coulter, Brea, CA, USA). The mean number of viable cells at varying concentrations of drug was normalized to the mean number of viable cells in the no-drug sample.

In vivo *experiments*
Twelve-week-old nude mice were injected with 5×10^5 cells of mixture of BaF3 cells expressing WT BCR–ABL and mutant forms of BCR–ABL (M244V, G250E, Q252H, Y253F, T315A, T315I, F317L, F317V, M351T and H396P). At 24-h injection of the leukemia cells, these mice were treated with either vehicle or AUY922 (50 mg/kg i.p.; two times per week) or nilotinib (30 mg/kg; q.d.) or AUY922 (50 mg/kg i.p.; two times per week) + nilotinib (30 mg/kg; q.d.). Mice were observed daily, and body weights as well as signs of stress (for example, lethargy, ruffled coat or ataxia) were used to detect possible toxicities.

Conflict of interest

TT receives research support from Novartis Pharma K.K.

Acknowledgements

This work was supported by a 'High-Tech Research Center' Project for private universities: matching fund subsidy from the MEXT (Ministry of Education, Culture, Sports, Science and Technology), and by the 'University-Industry Joint Research Project' for private universities: matching fund subsidy from the MEXT.

References

Azam M, Latek R, Daley GQ. (2003). Mechanisms of autoinhibition and STI-571/imatinib resistance revealed by mutagenesis of BCR-ABL. *Cell* **112**: 831–843.

Bantscheff M, Eberhard D, Abraham Y, Bastuck S, Boesche M, Hobson S *et al.* (2007). Quantitative chemical proteomics reveals mechanisms of action of clinical ABL kinase inhibitors. *Nat Biotech* **25**: 1035–1044.

Branford S, Melo JV, Hughes PT. (2009). Selecting optimal second-line tyrosine kinase inhibitor therapy for chronic myeloid leukemia patients after imatinib failure: does the BCR-ABL mutation status really matter? *Blood* **114**: 5426–5435.

Brough PA, Aherne W, Barril X, Borgogononi J, Boxall K, Cansfield JE *et al.* (2008). 4,5-Diarylisoxazole Hsp90 chaperone inhibitors: potential therapeutic agents for the treatment of cancer. *J Med Chem* **51**: 196–218.

Deguchi Y, Kimura S, Ashihara E, Niwa T, Hodohara K, Fujiyama Y *et al.* (2008). Comparison of imatinib, dasatinib, nilotinib and INNO-406 in imatinib-resistant cell lines. *Leuk Res* **32**: 980–983.

Eccles SA, Massey A, Raynaud FI, Sharp SY, Box G, Valenti M *et al.* (2008). NVP-AUY922: a novel heat shock protein 90 inhibitor active against xenograft tumor growth, angiogenesis, and metastasis. *Cancer Res* **68**: 2850–2860.

Garg RJ, Kantarjian H, O'Brien S, Quintas-Cardama A, Faderl S, Estrov Z *et al.* (2009). The use of nilotinib or dasatinib after failure to 2 prior tyrosine kinase inhibitors: long-term follow-up. *Blood* **114**: 4361–4368.

Gorre ME, Ellwood-Yen K, Chiosis G, Rosen N, Sawyers CL. (2002). BCR-ABL point mutants isolated from patients with imatinib mesylate-resistant chronic myeloid leukemia remain sensitive to inhibitors of the BCR-ABL chaperone heat shock protein 90. *Blood* **100**: 3041–3044.

Jabbour E, Kantarjian H, Jones D, Breeden M, Garcia-Manero G, O'Brien S *et al.* (2008). Characteristics and outcomes of patients with chronic myeloid leukemia and T315I mutation following failure of imatinib mesylate therapy. *Blood* **112**: 53–55.

Kano Y, Akutsu M, Tsunoda S, Mano H, Sato Y, Honma Y *et al.* (2001). In vitro cytotoxic effects of a tyrosine kinase inhibitor STI571 in combination with commonly used antileukemic agents. *Blood* **97**: 1999–2007.

Kantarjian H, Cortes J, Kim D-W, Dorlhiac-Llacer P, Pasquini R, DiPersio J *et al.* (2009). Phase 3 study of dasatinib 140 mg once daily versus 70 mg twice daily in patients with chronic myeloid leukemia in accelerated phase resistant or intolerant to imatinib: 15-month median follow-up. *Blood* **113**: 6322–6329.

Kantarjian H, Giles F, Wunderle L, Bhalla K, O'Brian S, Wassmann B *et al.* (2006). Nilotinib in imatinib-resistant CML and Philadelphia chromosome-positive ALL. *N Engl J Med* **354**: 2542–2551.

Kantarjian H, Pasquini R, Hamerschlak N, Rousselot P, Holowiecki P, Jootar S *et al.* (2007). Dasatinib or high-dose imatinib for chronic-phase chronic myeloid leukemia after failure of first-line imatinib: a randomized phase 2 trial. *Blood* **109**: 5143–5150.

Matsuyama W, Wang L, Farrar WL, Faure M, Yoshimura T. (2004). Activation of discoidin domain receptor 1 isoform b with collagen up-regulates chemokine production in human macrophages: role of p38 mitogen-activated protein kinase and NF-kappa B. *J Immunol* **172**: 2332–2340.

Nunoda K, Tauchi T, Takaku T, Okabe S, Akahane D, Sashida G *et al.* (2007). Identification and functional signature of genes regulated by structurally different ABL kinase inhibitors. *Oncogene* **26**: 4179–4188.

O'Hare T, Eide CA, Deininger MWN. (2007). Bcr-Abl kinase domain mutations, drug resistance, and the road to a cure for chronic myeloid leukemia. *Blood* **110**: 2242–2249.

Ottmann O, Dombret H, Martinelli G, Simonsson B, Guilhot F, Larson RA *et al.* (2007). Dasatinib induces rapid hematologic and cytogenetic responses in adult patients with Philadelphia chromosome positive acute lymphoblastic leukemia with resistance or intolerance to imatinib: interim results of a phase 2 study. *Blood* **110**: 2309–2315.

Ray A, Cowan-Jacob SW, Manley PW, Mestan J, Griffin JD. (2007). Identification of BCR-ABL point mutations conferring resistance to the Abl kinase inhibitor AMN107 (nilotinib) by a random mutagenesis study. *Blood* **109**: 5011–5015.

Rix U, Hantschel O, Dumberger G, Remsing Rix LL, Planyavsky M, Feenbach NV *et al.* (2007). Chemical proteomic profiles of the BCR-ABL inhibitors imatinib, nilotinib, and dasatinib reveal novel kinase and nonkinase targets. *Blood* **110**: 4055–4063.

Shah NP, Tran C, Lee FY, Chen P, Norris D, Saywers CL. (2004). Overriding imatinib resistance with a novel ABL kinase inhibitor. *Science* **305**: 399–401.

Stuhmer T, Zollinger A, Siegmund D, Chatterjee M, Grella E, Knop S *et al.* (2008). Signalling profile and antitumour activity of the novel Hsp90 inhibitor NVP-AUY922 in multiple myeloma. *Leukemia* **22**: 1604–1612.

Tauchi T, Boswell HS, Leibowitz D, Broxneyer HE. (1994). Coupling between p210bcr-abl and Shc and Grb2 adaptor proteins in hematopoietic cells permits growth factor receptor-independent link to ras activation pathway. *J Exp Med* **179**: 167–175.

Weisberg E, Manley PW, Breitenstein W, Bruggen J, Cowan-Jacob SW, Ray A *et al.* (2005). Characterization of AMN107, a selective inhibitor of native and mutant Bcr-Abl. *Cancer Cell* **7**: 129–141.

OPEN ACCESS Freely available online

PLoS one

15-Deoxy-$\Delta^{12,14}$ Prostaglandin J_2 Reduces the Formation of Atherosclerotic Lesions in Apolipoprotein E Knockout Mice

Takahiro Seno[1], Masahide Hamaguchi[2], Eishi Ashihara[3], Masataka Kohno[1], Hidetaka Ishino[1], Aihiro Yamamoto[1], Masatoshi Kadoya[1], Kaoru Nakamura[1], Ken Murakami[1], Satoaki Matoba[4], Taira Maekawa[5], Yutaka Kawahito[1]*

1 Department of Inflammation and Immunology, Graduate School of Medical Science, Kyoto Prefectural University of Medicine, Kyoto, Japan, **2** World Premier International Research Center, Immunology Frontier Research Center, Osaka University, Osaka, Japan, **3** Department of Molecular Cell Physiology, Graduate School of Medical Science, Kyoto Prefectural University of Medicine, Kyoto, Japan, **4** Department of Cardiovascular Medicine, Graduate School of Medical Science, Kyoto Prefectural University of Medicine, Kyoto, Japan, **5** Department of Transfusion Medicine and Cell Therapy, Kyoto University Hospital, Kyoto, Japan

Abstract

Aim: 15-Deoxy-$\Delta^{12,14}$ Prostaglandin J_2 (15d-PGJ_2) is a ligand of peroxisome proliferator-activated receptor γ (PPARγ) having diverse effects such as the differentiation of adipocytes and atherosclerotic lesion formation. 15d-PGJ_2 can also regulate the expression of inflammatory mediators on immune cells independent of PPARγ. We investigated the antiatherogenic effect of 15d-PGJ_2.

Methods: We fed apolipoprotein (apo) E-deficient female mice a Western-type diet from 8 to 16 wk of age and administered 1 mg/kg/day 15d-PGJ_2 intraperitoneally. We measured atherosclerotic lesions at the aortic root, and examined the expression of macrophage and inflammatory atherosclerotic molecules by immunohistochemical and real-time PCR in the lesion.

Results: Atherosclerotic lesion formation was reduced in apo E-null mice treated with 15d-PGJ_2, as compared to in the controls. Immunohistochemical and real-time PCR analyses showed that the expression of MCP-1, TNF-α, and MMP-9 in atherosclerotic lesions was significantly decreased in 15d-PGJ_2 treated mice. The 15d-PGJ_2 also reduced the expression of macrophages and RelA mRNA in atherosclerotic lesions.

Conclusion: This is the first report 15d-PGJ_2, a natural PPARγ agonist, can improve atherosclerotic lesions in vivo. 15d-PGJ_2 may be a beneficial therapeutic agent for atherosclerosis.

Citation: Seno T, Hamaguchi M, Ashihara E, Kohno M, Ishino H, et al. (2011) 15-Deoxy-$\Delta^{12,14}$ Prostaglandin J_2 Reduces the Formation of Atherosclerotic Lesions in Apolipoprotein E Knockout Mice. PLoS ONE 6(10): e25541. doi:10.1371/journal.pone.0025541

Editor: Massimo Federici, University of Tor Vergata, Italy

Received March 14, 2011; **Accepted** September 7, 2011; **Published** October 7, 2011

Funding: These authors have no support or funding to report.

Competing Interests: The authors have declared that no competing interests exist.

* E-mail: kawahity@koto.kpu-m.ac.jp

Introduction

Atherosclerosis is now recognized as a chronic inflammatory condition and remains the major cause of cardiovascular disease [1]. Over the past two decades, data have emerged showing that immune cells, especially macrophages, are involved in the formation of atherosclerotic plaques.

Peroxisome proliferator-activated receptor γ (PPARγ) is a member of the nuclear receptor superfamily, and is expressed in arterial wall cells, such as vascular smooth muscle cells, and macrophages [2]. Thiazolidinediones (TZDs), which are some of the most common PPARγ ligands, are insulin-sensitizing antidiabetic agents causing the improvement of hypertension and hypertriglyceridemia, both of which represent major risk factors for atherosclerosis. TZDs can improve atherosclerosis by decreasing these risk factors. A previous study indicated that troglitazone, a TZD, had pleiotropic anti-atherosclerotic effects on the expression of CD36 in atherosclerotic lesions and the serum level of HDL, but the details of the mechanisms were not clear [3]. Another function of TZDs comprises its anti-mitogenic effect on vascular smooth muscle cells [4]. TZDs also inhibit macrophage activation [5], monocyte migration [6], inflammatory cytokine secretion by monocytes [7–9], and the expression of cell adhesion molecules expressed by vascular endothelial cells [10,11]. Thus, a variety of anti-atherosclerotic effects of TZDs are associated with the regulation of inflammation caused by macrophages, but elucidation of the mechanisms in detail is required.

The J series of prostaglandins (PGs) have been demonstrated to regulate processes like inflammation and tumorgenesis [12]. 15-Deoxy-$\Delta^{12,14}$ Prostaglandin J_2 (15d-PGJ_2) is a metabolite of PGD_2, and is produced by mast cells, T cells, platelets and alveolar macrophages. 15d-PGJ_2 is recognized as an endogenous ligand for the intranuclear receptor PPARγ [13], which leads to inhibition of phorbol ester-induced nitric oxide and macrophage-derived

cytokines, i.e., tumor necrosis factor-α (TNF-α), IL-1 and IL-6. 15d-PGJ_2 inhibits gene expression in part by antagonizing the activities of transcription factors such as activator protein-1 and nuclear factor-κB (NF-κB) [7]. Furthermore, 15d-PGJ_2 has an anti-atherosclerotic effect as a ligand of PPARγ. Previous studies have been shown that 15d-PGJ_2 dose-dependently inhibits several functions of endothelial cells related to angiogenesis, such as proliferation, morphogenesis and migration in vitro [14–16]. Another study revealed that an increased plasma 15d-PGJ_2 concentration was associated with the early and late neurological outcomes, and a smaller infarct volume in ischemic stroke patients [17]. However, it remains unknown whether or not 15d-PGJ_2 has an anti-atherogenic effect in vivo. To investigate the effects of 15d-PGJ_2 on atherosclerotic lesion formation, we treated apo E–knockout mice, an animal model of atherosclerosis, with 15d-PGJ_2, and then examined the atherosclerotic lesions.

Methods

Animals

Apo E-knockout mice (C57BL/6J-Apoe^{tm1Unc}) were purchased from the Jackson Laboratory (B6 background; The Jackson Laboratory, Bar Habor, ME) [18]. These mice were produced by backcrossing the Apoe^{tm1Unc} mutation 10 times to C57BL/6J mice. Mice were maintained under specific pathogen-free conditions, and allowed ad libitum access to food and water. Thirty female animals aged 8 wk (15 as controls and 15 for the 15d-PGJ_2 experiments) were fed the Western-type diet containing 0.2% cholesterol and 21% saturated fat (Oriental Yeast, Tokyo, Japan) for 8 wk. All mice received intraperitoneal injections of (1) PBS (control group), and (2) 15d-PGJ_2 (Cayman Chemicals, Ann Arbor, USA), 1 mg/kg/day (15d-PGJ_2 group), for 8 wk with a high fat diet. Administration route and dosage of 15d-PGJ_2 were based on our previous study [19]. The animal care and experimental procedures conformed to the regulations of the Animal Research Committee, Graduate School of Medicine, Kyoto University.

Quantitative analyses of atherosclerotic lesions

Following blood collection, mice aged 16 wk treated with PBS or 15d-PGJ_2 were examined. After overnight fasting, blood was collected from the cardiac cavity and analyzed for the lipid profile. Also, aortae from the ascending portion to the end of the thoracic aorta were removed and washed meticulously in cold PBS to remove attached hematocytes and tissue fragments on the outside the aortae. Proximal aortic roots were used for quantitative analysis of the atherosclerotic area and whole thoracic aortae for real-time polymerase chain reaction (PCR) analysis.

Atherosclerotic lesions were quantitatively analyzed as previously described [20,21]. In brief, the basal portion of the heart and proximal aortic root were excised, embedded in OCT compound (Sakura Finetek, Tokyo, Japan), and then frozen in liquid nitrogen. Three serial cryosections per one aortic root of 10 μm thickness, at 40 μm intervals, of the aortic sinus were stained with oil-red O (Wako Pure Chemical Industries Ltd, Osaka, Japan) and hematoxylin. Other three cryosections per one aortic root were stained with Masson's trichrome (Kyodo Byori, Kobe, Japan) for cellular components (red) and fibrous tissue (blue). Lesion images were captured with a DMBA210 microscope (Shimadzu Rika, Tokyo, Japan) equipped with Motic Images Plus2.2s software (Shimadzu Rika, Tokyo, Japan). The captured images were analyzed with Image J software (NIH, USA). We calculated the oil-red O positive area, fibrotic area and aortic root area and compared the average data of three sections. A blind observer analyzed the lesions.

Immunohistochemistry

Immunohistochemistry was performed on 10 μm thick cryosections as described above. Tissue sections were immersed for 30 min in 0.3% hydrogen peroxide in methanol to block endogenous peroxidase activity. Nonspecific binding sites were saturated by exposure to 0.2% bovine serum albumin and normal serum for 30 min. Rat monoclonal anti-mouse macrophages (MOMA-2; AbD Serotec, Oxford, United Kingdom), goat anti-mouse monocyte chemoattractant protein-1 (MCP-1; Santa Cruz Biotechnology Inc., California, USA), rabbit anti-mouse macrophage migration inflammatory factor (MIF; Life Technologies, California, USA), goat anti-mouse TNF-α (R&D Systems, Minnesota, USA), goat anti-mouse matrix metallopeptidase-9 (MMP-9; Santa Cruz Biotechnology Inc., California, USA) and goat anti-mouse PPARγ (Santa Cruz Biotechnology Inc., California, USA) Abs were used as primary Abs. These primary anti-mouse macrophage Abs (1/50 dilution in PBS), anti-mouse MCP-1 Abs (1/100 dilution in PBS), anti-mouse MIF Abs (1/00 dilution in PBS), anti-mouse TNF-α Abs (1/100 dilution in PBS), anti-mouse MMP-9 Abs (1/100 dilution in PBS), anti-mouse PPARγ Abs (1/100 dilution in PBS) and control normal serum were applied to tissue sections, followed by incubation overnight at 4°C. The slides were treated with 0.2% glutaraldehyde. Then biotinylated secondary Abs and streptavidin–horseradish peroxidase were used for detection (Nichirei Bioscience, Tokyo, Japan) for 30 min. Signals were developed with a DAB Peroxidase Substrate Kit, 3,3′-diaminobenzidine (Vector Laboratories, Burlingame, USA). Positive staining was indicated by brownish black deposits, and counterstaining was performed with hematoxylin. The images were captured with a DMBA210 microscope, and the captured images were analyzed with Image J software (NIH, USA), the ratios of the positive area to the whole cross-sectional aortic wall area being calculated. Each data was average of three sections. A blind observer analyzed the lesions.

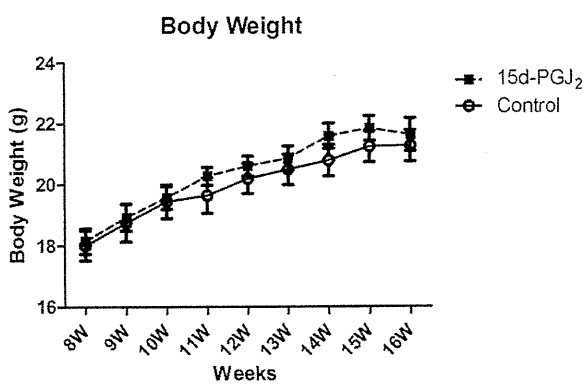

Figure 1. Body weights of apo E-knockout mice treated with PBS or 15d-PGJ_2 from 8 to 16 weeks of age. From the 8th week to 16th week, female mice were randomized to receive a Western-type diet and PBS or 1 mg/kg/day of 15d-PGJ_2 (n = 15 animals for each group). At 16th week, body weight of 15d-PGJ2 treated mice tended to be higher than controls, but it was not significantly different (21.6±4.2 g and 21.2±3.9 g, respectively, $p = 0.6$). Statistical analyses were performed with Student's t test.
doi:10.1371/journal.pone.0025541.g001

Real-time reverse-transcription polymerase chain reaction

Several gene expressions such as MCP-1, MIF, TNF-α, MMP-9 and RelA (p65), were analyzed by real-time quantitative RT-PCR using the TaqMan system based on real-time detection of accumulated fluorescence. Total RNA was extracted from whole thoracic aortae by homogenization in an RNeasy Fibrous Tissue Mini Kit (Qiagen Japan, Tokyo, Japan). cDNA was synthesized by reverse transcription with a Clontech Advantage RT-for-PCR Kit (Takara Bio Inc., Otsu, Japan). Quantitative real-time reverse-

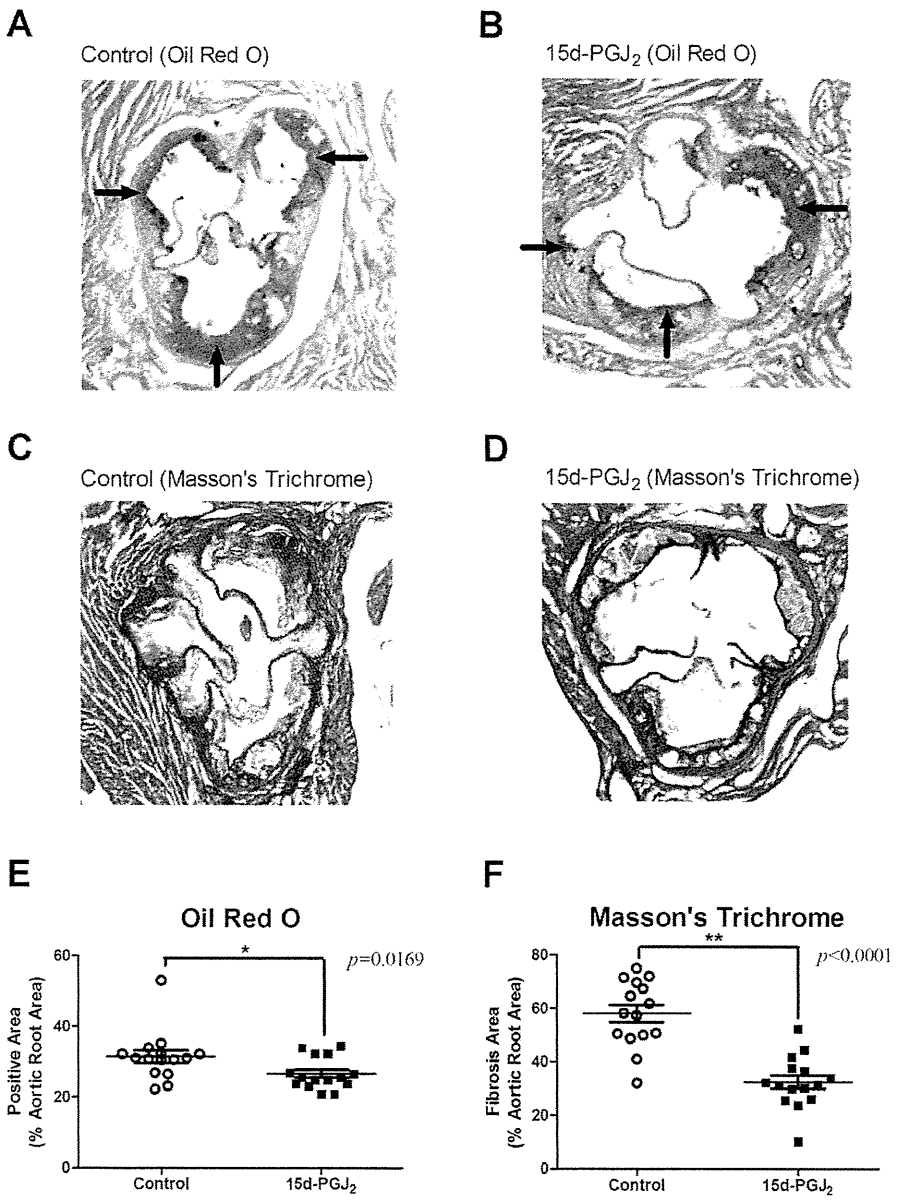

Figure 2. Representative oil red O stained sections and Masson's trichrome stained sections from the proximal aortae of apo E-knockout mice, and prevalence of atherosclerotic lesions. A and B are representative oil red O stained sections from the proximal aortae of apo E-knockout mice. C and D are representative Masson's trichrome stained sections. Apo E knockout-mice were fed a Western-type diet and treated with PBS (control group) (n = 15) (A, C) or 1 mg/kg/day 15d-PGJ_2 (15d-PGJ_2 group) (n = 15) (B, D) for 2 mo. Cross-sections of proximal aortae were stained with oil red O and counterstained with hematoxylin. Black arrows indicate the positive lesions. We plotted the prevalence of oil red O positive areas in cross-sections of whole atherosclerotic lesions in each group (E). Short lines indicate the means ± SD. The prevalence in controls were 31.44±1.811% and 26.63±1.169%, respectively. Cross-sections of proximal aortae were also stained with Masson's trichrome for cellular components (smooth muscle cells: pink, and red blood cells: red) and fibrous tissue (blue). We plotted the prevalence of fibrosis areas in cross-sections of whole atherosclerotic lesions in each group (F). Short lines indicate the means ± SD. The prevalence of fibrotic areas in controls were 58.05±3.218% and 32.48±2.535%, respectively. Statistical analyses were performed with Student's t test. *$p<0.05$, **$p<0.01$.
doi:10.1371/journal.pone.0025541.g002

transcription polymerase chain reaction was performed using an Applied Biosystems 7300 Real-Time PCR System (Applied Biosystems, California, USA), followed by analysis involving software detection system (SDS version 1.9) software. Gene expression was normalized as to 18S rRNA (Applied Biosystems).

Lipid metabolism

After overnight fasting, blood was collected from the cardiac cavity of mice aged 16 wk and analyzed for the lipid profile. The plasma chylomicron (CM), very low density lipoprotein (VLDL), low density lipoprotein (LDL), and high density lipoprotein (HDL) levels were determined by use of a high-sensitivity lipoprotein-profiling system by high-performance liquid chromatography (HPLC) (Skylight Biotech, Inc., Akita, Japan) [22]. HPLC with gel permeation columns was performed to classify and quantify lipoproteins on the basis of differences in particle size [23].

Statistical analysis

The results were expressed as means ± SE and analyzed by means of Student's t test (GraphPad Prism 5.03; Graph Pad Software Inc., CA, USA). Values of $p<0.05$ were considered statistically significant.

Results

Body weight

From the 8th week to 16th week, mice were randomized to receive a Western-type diet and PBS or 15d-PGJ_2. Figure 1 shows the change of body weight for observation period. At 16th week, body weight of 15d-PGJ_2 treated mice tended to be higher than controls, but it was not significantly different (21.6±4.2 g and 21.2±3.9 g, respectively, $p=0.6$). Body weight did not decrease after intraperitoneal administration of PBS or 15d-PGJ_2.

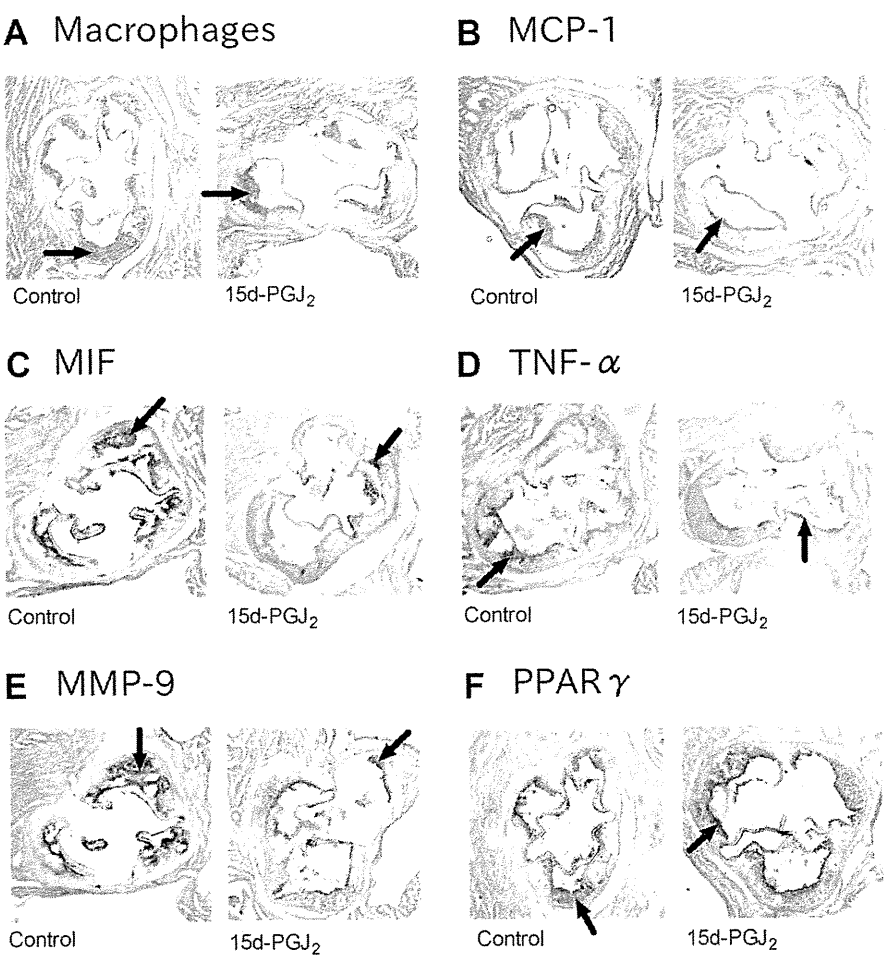

Figure 3. Representative sections with immunohistochemical analysis. Apo E-knockout mice were fed a Western-type diet and treated with PBS (control group) (n = 10) or 1 mg/kg/day 15d-PGJ_2 (15d-PGJ_2 group) (n = 10) for 2 mo. Representative cross-sections of the aortic sinus were stained with MOMA-2 (A), which detected macrophages, and MCP-1 Abs (B), MIF Abs (C), TNF-α Abs (D), MMP-9 Abs (E), PPARγ Abs (F), and counterstained with hematoxylin. Right sections are control group and left ones are 15d-PGJ_2 group in each figure. Black arrows indicate the positive lesions.

doi:10.1371/journal.pone.0025541.g003

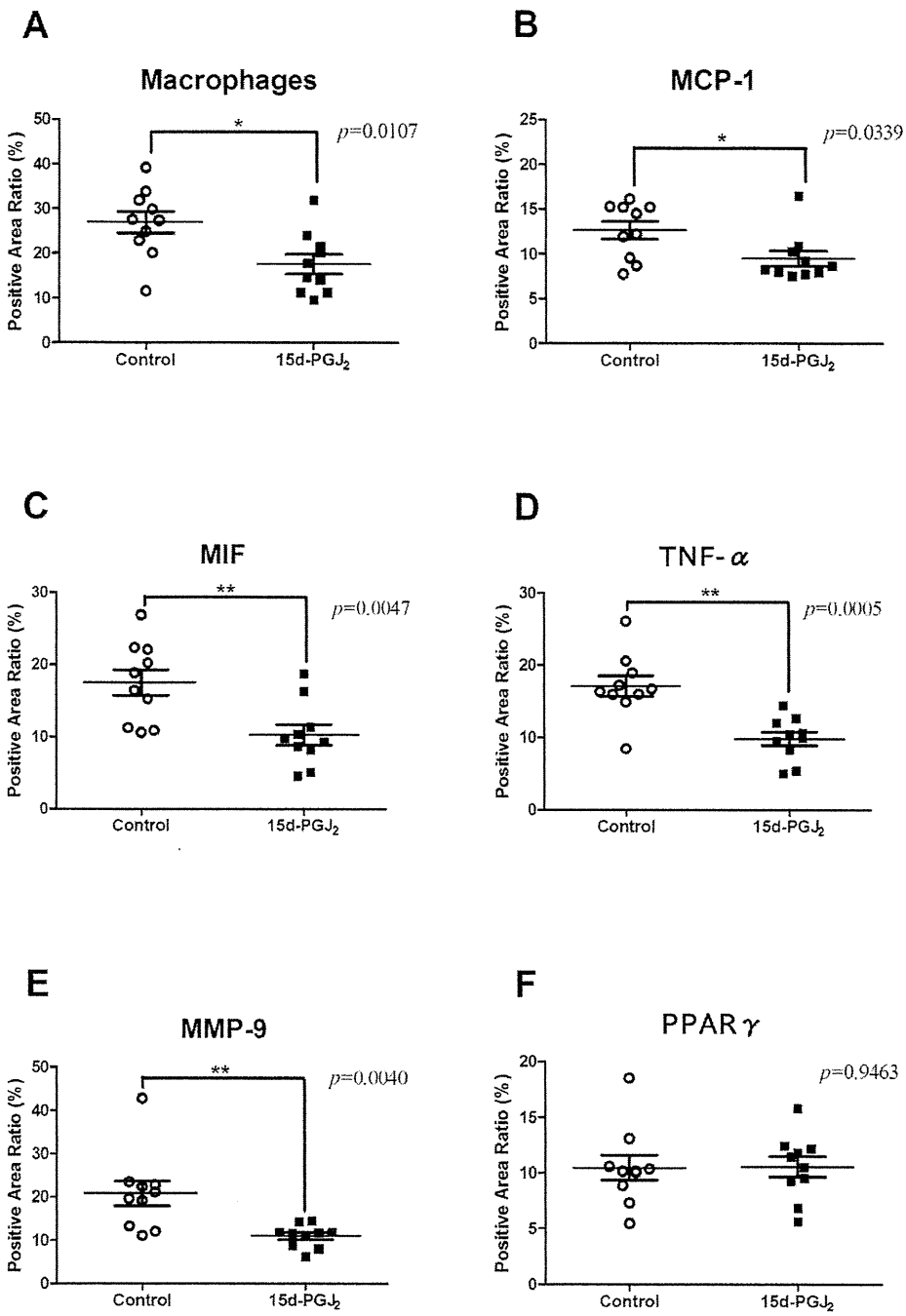

Figure 4. Prevalence of atherosclerotic lesions with immunohistochemical analysis. Apo E-knockout mice were fed a Western-type diet and treated with PBS (control group) (n = 10) or 1 mg/kg/day 15d-PGJ_2 (15d-PGJ_2 group) (n = 10) for 2 mo. Representative cross-sections of the aortic sinus were stained with MOMA-2, which detected macrophages, and MCP-1 Abs, MIF Abs, TNF-α Abs, MMP-9 Abs, PPARγ Abs, and counterstained with hematoxylin. We plotted the prevalence of positive areas in cross-sections of whole atherosclerotic lesions in each group. Short lines indicate the means ± SD. The prevalence of macrophage (A), immunoreactive MCP-1 (B), MIF (C), TNF-α (D) and MMP-9 (E) in atherosclerotic lesions of apo E-knockout mice treated with PBS or 15d-PGJ2 was examined. The prevalence of macrophage in the control and 15d-PGJ_2 groups were 26.97±2.437% and 17.64±2.194%, respectively. The prevalence of immunoreactive MCP-1 (9.508±0.8518% vs 12.65±0.9788%, $p = 0.0339$), MIF (10.28±1.402% vs 17.53±1.762%, $p = 0.0047$), TNF-α (9.853±0.9462% vs 17.12±1.412%, $p = 0.0005$) and MMP-9 (11.02±0.8208% vs 20.80±2.846%, $p = 0.0040$) were decreased in the 15d-PGJ_2 groups. But the prevalence of PPARγ (F) was not different between both groups (10.55±0.9217% vs 10.46±1.104%, $p = 0.9463$). *$p<0.05$, **$p<0.01$, with Student's t test.
doi:10.1371/journal.pone.0025541.g004

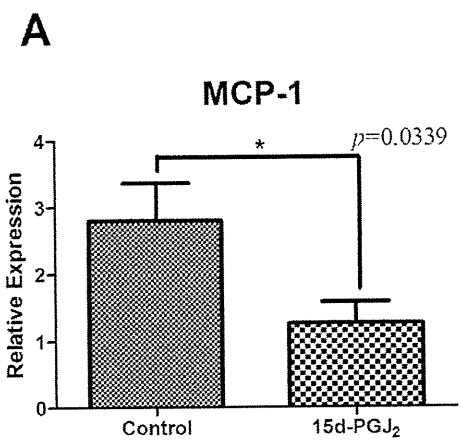
A
MCP-1
Relative Expression
*
p=0.0339
Control
15d-PGJ2

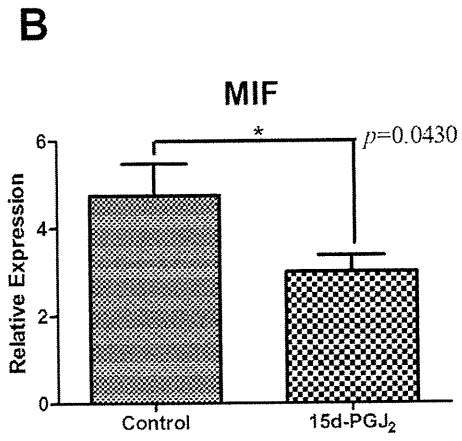
B
MIF
Relative Expression
*
p=0.0430
Control
15d-PGJ2

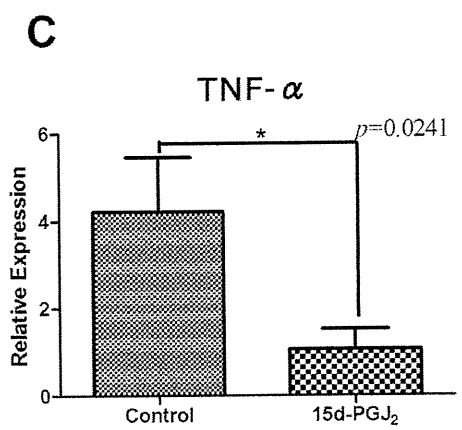
C
TNF-α
Relative Expression
*
p=0.0241
Control
15d-PGJ2

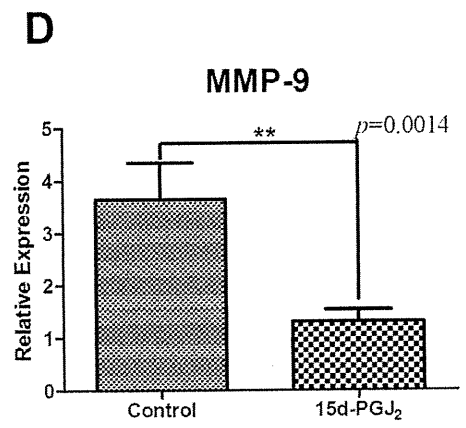
D
MMP-9
Relative Expression
**
p=0.0014
Control
15d-PGJ2

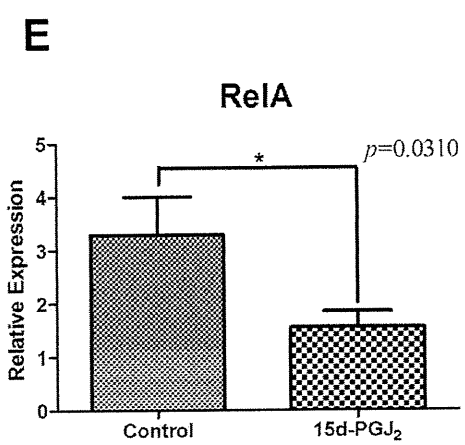
E
RelA
Relative Expression
*
p=0.0310
Control
15d-PGJ2

Figure 5. Comparison of gene expressions in the thoracic aorta between the control and 15d-PGJ$_2$ treated groups by real-time PCR analysis. Apo E-knockout mice were fed a Western-type diet and treated with PBS (control group) or 1 mg/kg/day 15d-PGJ$_2$ (15d-PGJ$_2$ group) for 2 mo. Thoracic aortae were removed and total RNA was extracted from them. cDNA was synthesized by reverse transcription, and quantitative real-time PCR was performed. The relative gene expression values were calculated. The relative expressions were significantly decreased in the 15d-PGJ$_2$ group, MCP-1 (1.263±0.3193 vs 2.802±0.5627, $p=0.0339$) (A), MIF (2.985±0.3860 vs 4.745±0.7347, $p=0.0430$) (B), TNF-α (1.059±0.4625 vs 4.220±1.236, $p=0.0241$) (C), MMP-9 (1.304±0.2344 vs 3.644±0.6947, $p=0.0014$) (D) and RelA (1.551±0.2995 vs 3.294±0.7093, $p=0.0310$) (E), compared with in the control group. *$p<0.05$, **$p<0.01$, with Student's t test.
doi:10.1371/journal.pone.0025541.g005

Atherosclerotic lesions in the aortic sinus

To determine the factors mediating the anti-atherosclerotic effect of 15d-PGJ$_2$, we compared the area of oil red O-positive lesions and fibrotic lesions in cross-sections of the aortic wall between the control and 15d-PGJ$_2$ groups (n = 15, respectively). Representative micrographs are presented in Figure 2. Typical atheromas with well-developed, lipid-rich cores and foam cell infiltration were observed. The prevalence of oil red O positive areas in cross-sections of whole atherosclerotic lesions were 31.44±1.811% in the controls and 26.63±1.169% in the 15d-PGJ$_2$ groups. The prevalence of Masson's trichrome stained fibrotic areas were 58.05±3.218% and 32.48±2.535%, respectively.

Immunohistochemistry of the atherosclerotic lesions

We explored the mechanism underlying the anti-atherosclerotic effect of 15d-PGJ$_2$. Immunohistochemistry was performed with MOMA-2, which detected macrophages, anti-MCP-1 Abs, anti-MIF Abs, anti- TNF-α Abs, and anti-MMP-9 Abs. We compared the prevalence of positive areas in the aortic root between the control and 15d-PGJ$_2$ groups (n = 10, respectively). The 15d-PGJ$_2$ group exhibited significant lower expression of MCP-1 (9.508±0.8518% vs 12.65±0.9788%, $p=0.0339$), MIF (10.28±1.402% vs 17.53±1.762%, $p=0.0047$), TNF-α (9.853±0.9462% vs 17.12±1.412%, $p=0.0005$), MMP-9 (11.02±0.8208% vs 20.80±2.846%, $p=0.0040$) and macrophages (17.64±2.194% vs 26.97±2.437%, $p=0.0107$), compared with in control group (Figure 3A–3E, Figure 4A–4E). But the prevalence of PPARγ was not different between both groups (10.55±0.9217% vs 10.46±1.104%, $p=0.9463$) (Figure 3F, Figure 4F).

Gene expressions in the thoracic aorta

Figure 5 shows the results of quantitative real-time PCR analysis of MCP-1, MIF, TNFα, MMP-9 and RelA gene expressions in thoracic aortae. All of those gene expressions were significantly decreased in the 15d-PGJ$_2$ group (n = 10, respectively), MCP-1 (1.263±0.3193 vs 2.802±0.5627, $p=0.0339$), MIF (2.985±0.3860 vs 4.745±0.7347, $p=0.0430$), TNF-α (1.059±0.4625 vs 4.220±1.236, $p=0.0241$), MMP-9 (1.304±0.2344 vs 3.644±0.6947, $p=0.0014$) and RelA (1.551±0.2995 vs 3.294±0.7093, $p=0.0310$), compared with in the control group. 15d-PGJ$_2$ also reduced the expressions of these atherosclerotic markers at the gene level. It indicated that 15d-PGJ$_2$ led to downregulation of these gene expressions via NF-κB, and these results were almost comparable with immunohistochemistry. In addition, ligand-induced negative-feedback was not identified in our study.

15d-PGJ$_2$ treatment improves the lipid profile

We performed analyses of lipid levels at the end of this study. Pooled plasma from all mice was subjected to HPLC. Lipoproteins were separated in CM, VLDL, LDL, and HDL. The total serum cholesterol level was significantly lower in the15d-PGJ$_2$ group than in the control group (795.5±39.31 mg/dl vs 944.1±49.04 mg/dl, $p=0.029$) (Figure 6A). Especially LDL was significantly reduced in the 15d-PGJ$_2$ group (186.9±13.49 mg/dl vs 234.3±16.60 mg/dl, $p=0.0397$) (Figure 6D). CM and VLDL tended to be lower than in controls, but the difference was not significant (36.96±4.999 mg/dl vs 68.13±23.98 mg/dl, p = 0.1415; 553.5±26.67 mg/dl vs 622.7±28.02 mg/dl, $p=0.1005$, respectively) (Figure 6B and C). The HDL level was not different between the control and 15d-PGJ$_2$ groups (18.14±1.264 mg/dl vs 19.01±2.562 mg/dl, $p=0.7413$) (Figure 6E).

Discussion

15d-PGJ$_2$ is a ligand of PPARγ, which acts to atherosclerosis formation. In this study, we fed apo E-deficient mice a Western-type diet and administered 15d-PGJ$_2$. We measured the cross-sectional atherosclerotic area in the proximal aorta and examined the expression of several atherosclerotic markers in the lesions. The atherosclerotic area, represented by lipid accumulation and fibrous tissue, significantly decreased in apo E-null mice treated with 15d-PGJ$_2$. Immunohistochemical and real-time PCR analyses showed that the expressions of MCP-1, MIF, TNF-α and MMP-9 in atherosclerotic lesions were significantly decreased. The 15d-PGJ$_2$ also reduced the expression of RelA mRNA in atherosclerotic lesions. This study suggests that 15d-PGJ$_2$ has an anti-atherosclerotic effect.

Atherosclerosis is an inflammatory disease. The lesions in atherosclerosis represent a series of highly specific cellular and molecular responses that can best be described, overall, as an inflammatory disease [24]. Atherosclerosis formation consists of several steps. The earliest changes that precede the formation of lesions of atherosclerosis take place in the endothelium. These changes include migration of leukocytes into the artery wall, which is mediated by MCP-1 [24]. Fatty streaks initially consist of lipid-laden monocytes and macrophages together with T lymphocytes. Later they are joined by various numbers of smooth-muscle cells. The steps involved in this process include T cell activation, foam-cell formation, which is mediated by TNF-α. As the advanced change, thinning of the fibrous cap is apparently due to the continuing influx and activation of macrophages, which release metalloproteinases such as MMP-9, and other proteolytic enzymes at these sites. MIF affects cell proliferation in lesions and elastolytic/collagenolytic cysteine protease expression. MIF may act as do other cytokines (eg, TNF-α) to enhance protease expression and vascular cell proliferation, processes that occur during atherogenesis [25]. Our data showed that 15d-PGJ$_2$ inhibited MCP-1, MIF, TNF-α and MMP-9 as indicated by real-time PCR as well as immunohistochemical analysis. A previous study showed that thiazolidinediones and 15d-PGJ$_2$ inhibit macrophage proliferation in a dose-dependent manner, and significantly reduce the migration of monocytes induced by MCP-1 in vitro [26]. Also, MCP-1 is one of the important mediators at early change of atherosclerosis formation. On possibility is that 15d-PGJ$_2$ act on various steps of atherosclerosis formation. Another possibility is that 15d-PGJ$_2$ act on the early step of atherosclerosis formation, as a consequence, 15d-PGJ$_2$ decrease the mediators at following steps.

15d-PGJ$_2$ is one of the PPARγ-ligands [13] emerging as a key anti-inflammatory mediator via NF-κB inhibition, may play a role in the pathogenesis of atherosclerosis [2]. NF-κB family consists of